The Thesis Committee for Lauren Violet Milisits
Certifies that this is the approved version of the following thesis:

Methodology for Mechanical Property Optimization of Selective Laser Sintered Parts Using Design of Experiments

APPROVED BY
SUPERVISING COMMITTEE:

Supervisor: _____
Dragan Djurdjanovic

Co-Supervisor: _____
David L. Bourell

Methodology for Mechanical Property Optimization of Selective Laser Sintered Parts Using Design of Experiments

by

Lauren Violet Milisits, B.S. Mech. Engr.; B.S. Comp. Sci.

Thesis

Presented to the Faculty of the Graduate School of

The University of Texas at Austin

in Partial Fulfillment

of the Requirements

for the Degree of

Master of Science in Engineering

The University of Texas at Austin

May 2017

Dedication

To my parents, thank you for encouraging my dream as a child to be an astronaut and for instilling in me a love for science and engineering.

To Ryan and Lindsey, thank you for all of your love and support over the years. I am thankful to have such a wonderful and caring brother and sister.

To Campbell, thank you for being a supportive best friend. I remember my first visit to explore the Mechanical Engineering building at UT, and walking around with you in awe of what the next two years would bring.

And to Francisco, thank you for your endless support to pursue my graduate studies dream. Thank you for all of the miles and hours and trips to visit me in Austin. Most of all, thank you for always being there. Your love and encouragement has meant everything to me.

I love you all.

Acknowledgements

The work presented within this thesis would not have been possible without the multitude of people who guided me through my research in one form or another. I would first like to express my sincere gratitude to each of my advisors, Dragan Djurdjanovic and David L. Bourell. The support and encouragement from each has provided me with an incredible research experience, and I would not have been able to complete this work without their guidance.

This hands-on research required the use of multiple labs for experimentation and testing. I would like to thank Mark Phillips, Abhimanyu Bhat, Vikram Devaraj and Will Scharnberg for all of their help in the sintering lab including training me on the machine and answering all of my questions to ensure that my builds were successful. I want to thank Jared Allison and Christopher Roberts for their help with the tensile testing machine. Thank you to Rich Piner for training me on the optical profilometer. Additionally, thank you to Stratasys Direct Manufacturing and Chris Heinze for allowing me to use the density testing equipment in Belton.

Finally, thank you to Spiceworks, Leigh Sullivan and Blake Lusenhop for the continued support these past two years.

Abstract

Methodology for Mechanical Property Optimization of Selective Laser Sintered Parts Using Design of Experiments

Lauren Violet Milisits, M.S.E.

The University of Texas at Austin, 2017

Supervisor: Dragan Djurdjanovic

Co-Supervisor: David L. Bourell

Selective laser sintering (SLS) is a form of additive manufacturing progressively used to manufacture end-use parts for industries including aerospace, automobile and biomedical. Machine settings, laser settings, and powder properties are all input parameters that affect the dimensional quality and mechanical properties of the produced SLS parts. A key challenge to successfully manufacturing SLS parts is learning how to control these parameters and finding the optimal settings such that desired mechanical properties are robustly achieved. This thesis proposes a design of experiments (DOE) based methodology to optimize mechanical properties of SLS parts. The study performs a DOE on three design variables (fill laser power, outline laser power, scan spacing) with three levels and measures six response variables (tensile strength, tensile modulus, tensile elongation-at-break, density, hardness, surface roughness). Experiments are performed using a work material of ALM PA 650 unfilled nylon 12 performance polyamide blend. The effects of the selected parameters on different part quality metrics are analyzed and discussed. A confirmatory test to prove the optimized model is performed and evaluated.

Table of Contents

List of Tables

List of Figures

Chapter 1: Introduction

1.1 Selective laser sintering background

Selective laser sintering (SLS) is an additive manufacturing (AM) process invented by Carl Deckard at the Mechanical Engineering Department of the University of Texas at Austin. Deckard filed the first patent for his research in October 1986 [1], and SLS became the first commercialized powder bed fusion (PBF) process [2, p. 107].

The SLS process consists of three stages: warm-up, build and cool-down. During the *warm-up* stage, feed cartridges are first filled with the powdered material and the build platform is primed with a layer (typically 1-2 inches) of powder. The machine is then pre-heated for approximately 2 hours to a temperature just below the melting point for the specific powdered material [2, p. 108].

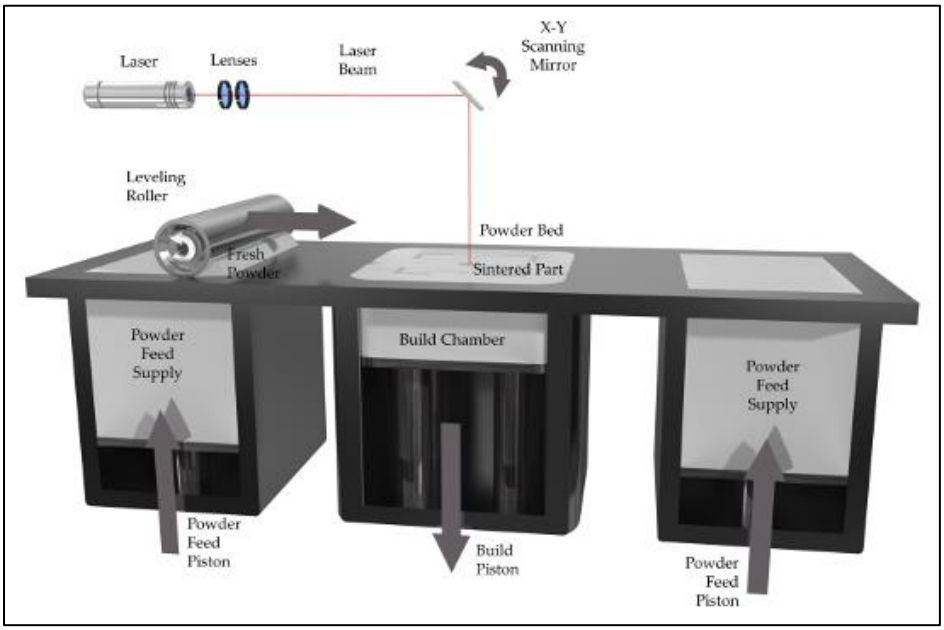

Figure 1: Illustration of the SLS process [3]

During the *build* stage, a CO_2 laser beam selectively scans the powder bed to form the first layer of the part. The laser outlines the cross-section of the part, which is obtained from the stereolithography (STL) file, and then scans the interior of the cross-section to fill-in and complete the layer. When the layer is completed, the build platform is lowered by one layer thickness, and a counter-rotating leveling roller (Figure 1) applies a fresh layer of powder. Excess powder is collected in over-flow containers on each side of the machine, and the laser scans the cross-section of the new layer. The process is repeated until the part is completed [2, pp. 4-5, 108].

The final step of the SLS process is the *cool-down* stage. The powder bed is slowly cooled before removing the part from the machine to avoid warping. When the powder bed has cooled, the solid SLS part and part cake are removed from the build chamber. The SLS part is separated from the part cake and then air blasted to clean off excess powder. The manufactured part may go through subsequent post-processing, while the part cake and powder from the over-flow chamber may be recycled for future use [2, pp. 6, 108-109].

SLS is an emerging technology for manufacturing developed relatively recently[1]. However, the use of SLS as a manufacturing method for prototypes and end-use parts can be advantageous. Parts with complex geometries, for which previously multiple iterative processes may have been needed with a skilled craftsmen employing a variety of construction methods, can now be crafted in a single stage using SLS. The loose, unsintered powder acts as a natural support structure throughout the build process allowing for parts to be oriented in any direction within the build chamber, and the unsintered powder is easily removed by air blasting during post-processing [2, pp. 9-12, 143].

[1] The earliest processes for injection molding were patented nearly 145 years ago in 1872 [34].

Although SLS technology continues to make advancements, it should be noted that there are still many issues regarding process control that hinder it from becoming more commonplace. The mechanical and surface properties of parts manufactured using SLS are dependent upon a variety of process parameters, and little effort has been made to understand the relationship between these parameters and the mechanical and surface properties of the finished part. Despite executing builds with identical process parameters, the repeatability of part quality metrics can vary widely within and between identical builds. While SLS manufacturers "implement stringent, proprietary process controls and procedures" in an effort to ensure consistent build quality, this undisclosed information is intellectual property to the company and what allows the commercialized manufacturers to remain competitive in the industry [4]. As a result, there is a lack of public and standardized information for the idyllic process parameter settings to achieve the desired mechanical properties of SLS parts made from assorted sintering materials on distinct SLS machines.

1.2 RESEARCH OBJECTIVES

The efforts of this thesis aim to propose an experimental methodology to optimize mechanical properties of parts built using SLS technology and to successfully demonstrate an application of the methodology. In theory, the proposed methodology can be replicated on any SLS powdered material, on any machine, with any number of selected processing parameters, and can be used to optimize any number of desired mechanical properties. In this thesis, to successfully develop and apply the methodology, the research has the following objectives:

1. To use a DOE on three design variables with three levels each (3^3 degrees-of-freedom) in order to build test specimens

2. To collect data for six selected responses from the test specimens to build a set of experimental data
3. To analyze the data in order to determine the effects of each design variable on the responses
4. To develop a model of best fit for each response from the experimental data
5. To estimate the experimental noise characteristics via analysis of variance (ANOVA)
6. To demonstrate applicability of the proposed DOE based optimization by performing confirmatory tests with the response models

1.3 ORGANIZATION OF THESIS

The thesis is structured into five chapters. The current chapter briefly discusses the background of SLS and introduces the motivation and objectives for the research. The "Literature review" chapter motivates the research objectives by analyzing previous efforts to investigate SLS process parameters and optimize mechanical properties. The "Methods" chapter discusses the detailed methodology to experimentally optimize mechanical properties of SLS parts and gather data from the test specimens. The "Results and discussion" chapter analyzes the data obtained from the test specimens, builds a model to optimize the response variables, and performs a set of experiments to validate the models. The final chapter provides a summary and conclusions of the research and suggestions for future work.

Chapter 2: Literature Review

2.1 Characterizing process parameters

Over the last thirty years, since the SLS process was first invented and patented, several research advancements have been made. Initial work was completed to correlate process parameters to area energy density. To characterize area energy density, ED_A – also referred to as the Andrew Number, A_N – delivered to the powder bed, Nelson [5] developed the simplified model given in Equation 1:

$$ED_A = \frac{P}{V * HS} \tag{1}$$

where ED_A is in [J/m^2], P is the laser power in [W], V is the velocity of the laser beam in [m/s], and HS is the hatch (or scan) spacing of the laser in [m]. This equation was further expanded upon by Starr *et al.* [6] [7] in order to illustrate volume energy density. The resulting model is given in Equation 2:

$$ED_V = \frac{P}{V * HS * \lambda} \tag{2}$$

where ED_V is in [J/m^3] and λ is the layer thickness [m]. The energy density equations can be used to relate physical properties of parts to the independent process parameters [8]. Bourell *et al.* [9] showed that of the different energy density equations available, volume energy density (Equation 2) best correlates to the resulting mass density and tensile strength for SLS parts manufactured from polyamide 12.

Several publications discuss research efforts to correlate process parameters to mechanical properties of SLS parts. Gibson and Shi [10] experimented on a Sinterstation 2000 with a fine nylon material and altered fill laser power, scan size, scan spacing and part orientation to correlate these parameters to the tensile strength and density of the SLS parts. They found that with increasing fill laser power, tensile strength and part density have a limiting value and concluded that an optimal value for energy density may exist.

They did not, however, suggest a method to determine the optimum. Gibson and Shi also showed that parts built in the Z-axis orientation have the worst tensile strength; this is due to the force being applied in the build layer direction.

Starr *et al.* [7] experimented with nylon 12 on a Sinterstation 2500^{plus}. Their research further concluded that at lower power levels, all parts have reduced tensile strength regardless of the build orientation. However, as power levels increase to an intermediate level, part orientation begins to have a significant effect on tensile strength, echoing the results of Gibson and Shi. Starr *et al.'s* analysis further expands upon these findings – given that a part is oriented length-wise in the Z-axis, the orientation of the width of the part along the Z-X or Z-Y axis does have a significant effect on the part's tensile strength.

Additional analysis to correlate processing parameters has been conducted by many researchers. Ho *et al.* [11] correlated the tensile strength and part density of polycarbonate SLS parts as a function of energy density. Zarringhalam *et al.* [12] studied potential sources of the lack of reproducibility of SLS parts and related the results to various mechanical properties. However, this research was limited and focused on two experiments performed on separate machines with different processing parameters for each machine, making it difficult for the results to correlate to specific effects. Additional technical literature demonstrates similar drawbacks in that they do not fully explore a range of processing parameters. Majewski and Hopkinson [13] concluded that layer thickness and orientation did not affect tensile strength, but the experiments did not vary other processing parameters. Caulfield *et al.* [14] explored the effects of increasing laser power (energy density) on part strength and apparent density, but the experiments were conducted with constant scan spacing. Finally, Choren *et al.* [15] explored the effects of various

mechanical properties at three levels of fill laser power but a constant level for scan spacing and scan speed.

2.2 Optimization attempts and limitations

There are several technical literature sources that have emerged in recent years that implore a DOE based methodology. Some researchers have used DOE to better understand the effects of specific processing parameters. For example, Savalani *et al.* [6] performed a two-level full factorial DOE on hydroxyapatite-polymer composite material to identify the effects of layer thickness, laser power, scan spacing and scan speed on porosity, pore size and channel width – crucial bio-application outputs.

Other researchers have applied a DOE method in order to optimize a specific part quality metric, and it appears that most of these efforts are focused only on optimizing part density. Liao *et al.* [16] performed a two-level fractional factorial DOE with replications on a metallic nickel powder to identify the effects of particle size, pulse frequency, pulse duration and number of pulses on the porosity of the SLS part. Similarly, Chung *et al.* [17] investigated glass-filled nylon 11 specimens with a two-level factorial DOE on five processing parameters to determine optimal values for maximized part density. Lastly, Liu *et al.* [18] utilized a three-level DOE on dental glass-ceramics powder to explore the effects of laser power, scan spacing and scan speed on relative density and bending strength. Using a linear regression model, optimal processing parameters were determined to increase the relative density.

While there have been some efforts to conduct a three-level DOE based study and to build a model of the optimal response, there were limitations with the research. Singh *et al.* [19] developed a quadratic model to model sintered part density based on a mathematical model and using finite element analysis. After the model was determined, no

physical experimentation was conducted to validate the model, rather, the optimal results were compared to literature sources. Again, as seen in the previous technical literature, only one part quality metric was examined – density.

The literature review shows that there has been some research efforts aimed to characterize processing parameters and their effects on mechanical properties of SLS parts. However, this research is often limited in scope to exploring the effects of varying a single processing parameter while holding all others constant. Further, the mechanical property most often explored is sintered part density or porosity with little effort to explore other mechanical properties such as hardness, fracture toughness, impact strength or surface roughness. Another finding from the literature review is that there have been attempts to optimize a single part quality metric, but at times, only a linear model is developed. The issue from this is that a true optimum is not determined, but rather a value *near* the optimum is found [20].

The purpose of this thesis will expand upon current research to investigate a reproducible methodology to explore the effects of any processing parameter on any desired number of mechanical properties with any selected work material. Further, it is also the purpose of this thesis to develop a model to optimize the selected mechanical properties and to demonstrate validity of the models for any mechanical property.

Chapter 3: Methods

The methodology proposed aims to demonstrate optimization of mechanical properties of laser sintered parts. It is first necessary to select the processing parameters of importance, along with the working range of values to be experimented upon, in order to measure the selected response variables. Consideration should be given as to what test specimens, or parts, should be built in order to measure the response variables. An experimentation model most appropriate for the analysis is selected, and then the design matrix can be developed. The experiments should be conducted according to the design matrix in randomized order on the selected work material for processing. After experimentation is performed, data will be gathered from the test specimens to measure the response variables, and the responses will be analyzed using analysis of variance (ANOVA). Finally, with response models obtained from the experimental data, values for all process parameters are determined to optimize each response variable, and a confirmatory test to demonstrate proof of the model will be conducted. An application of the methodology sequence is discussed and demonstrated below.

3.1 PROCESS PARAMETERS

3.1.1 Selection of process parameters

The machine process parameters, or design variables, selected for experimentation are fill laser power, outline laser power, and scan spacing. These parameters were selected based on prior research demonstrating that laser power and scan spacing affect the energy density supplied to the powder material [21]. As discussed in the literature review, laser power and scan spacing have a direct impact on the energy density of the sintered part, thus directly affecting the mechanical properties selected as response variables.

3.1.2 Range of values for process parameters

The range of values for the process parameters were selected and determined based on expert knowledge and experience with the chosen work material and in such a way that optimal settings for the process are expected within those ranges. The working range of the selected process parameters are shown in Table 1. The table also includes the coded, dimensionless levels for the DOE, shown in bold. The 0-level represents the current setting at which the SLS machine is typically operated at in order to manufacture Nylon 12 parts.

Parameter		**-1**	**0**	**+1**
$\mathbf{X_1}$	Fill laser power, *W*	20	24	28
$\mathbf{X_2}$	Outline laser power, *W*	3	5	7
$\mathbf{X_3}$	Scan spacing, *in*	0.006	0.010	0.014

Table 1: Selected process parameters and encoding of values

3.2 RESPONSE VARIABLES AND TEST METHODS

The response variables of interest for this study were the following mechanical properties: tensile strength, tensile modulus, elongation-at-break, sintered part density, hardness, and surface roughness. Table 2 summarizes the response variables and selected test methods for each property. The ALM Material Processing Guide [22] lists typical physical properties and the test methods used to determine the metric values; these test methods were adopted to evaluate the selected response variables in this thesis.

	Response	Test Method	Specimen
Y_1	Ultimate tensile strength (XY)	ASTM D638 [23]	Type I tensile bar
Y_2	Tensile modulus (XY)	ASTM D638 [23]	Type I tensile bar
Y_3	Tensile elongation-at-break	ASTM D638 [23]	Type I tensile bar
Y_4	Sintered part density	ASTM D792 [24]	1” x 1” x 1” cube
Y_5	Hardness (Shore D)	ASTM D2240 [25]	1” x 1” x 1” cube
Y_6	Surface roughness	Laser diffraction	2.5” x 0.5” x 0.125” bar

Table 2: Selected response variables and test methods

3.3 CONTROL VARIABLES IN THE EXPERIMENTS

The control variables are machine process parameters and other variables that were kept constant throughout the experiments to reduce the noise measured in the response variables. All experiments were performed by the same individual to reduce operator noise. Table 3 summarizes the control variables for this study.

Parameter	Value
Machine Settings	
Layer thickness	100 µm
Roller speed	10 in/s
Preheat temperature	
Left/Right feed	140 °C
Part bed	174 °C
Warm-up time	1 hour 45 mins
Cool-down time	6 hours
Laser Settings	
Type	CO_2
Fill beam offset	
X	0.01 in
Y	0.01 in
Scanning speed	
Fill	400 in/s
Outline	70 in/s
Scan count	
Fill	1
Outline	1
Powder Properties	
Material	ALM PA 650 Unfilled Nylon 12 [22]
Particle size	55 µm
Mixture	30% fresh powder
	70% recycled powder
	35% part cake
	35% overflow

Table 3: Control parameters and values

3.4 EXPERIMENTAL MODEL

3.4.1 Design of experiments

The model was developed using a design of experiments (DOE) based methodology. A DOE is a scientific approach to systematically change the levels of input variables such that the effects of the design variables can be correlated to the observed

responses [26]. For this study, three process parameters were selected with three levels for experimentation and six response variables were measured.

3.4.2 Design of experiment runs

The goal of the proposed methodology is to develop a model of best fit such that the desired response variables can be optimized. The demonstrated methodology in this thesis will develop a quadratic model of best fit for each response variable because a quadratic model is the simplest model that can represent curvature of the response surface; in order to detect curvature, three levels of the factors are needed [20]. The quadratic model will have the following form:

$$y = \beta_0 + \beta_1 x_1^2 + \beta_2 x_2^2 + \beta_3 x_3^2 + \beta_4 x_1 x_2 + \beta_5 x_1 x_3 + \beta_6 x_2 x_3 + \beta_7 x_1 + \beta_8 x_2 + \beta_9 x_3$$

where $x_1, x_2, \text{and } x_3$ are the selected process parameters and β_i are coefficients representing the effect of the variables and interactions.

A minimum of 10 experiments are required to solve for the 10 unknowns; however, additional experiments provide supplementary data to better fit the model. For this thesis, 21 experiments were conducted. The experimental design focused on the 8 edge points of a cube, the 8 midpoints of a cube and a center point within a cube.

The experiments were performed in random order (run order) to eliminate bias from being introduced into the measured responses. Table 4 summarizes the experiment runs, the run order, the levels of each design variable for each experimental trial, and the corresponding energy density of each trial. Volume Energy density is calculated with Equation 2.

Standard Order	Run Order	X_1	X_2	X_3	Energy Density J/mm^3
1	2	-1	-1	-1	5.080
2	7	-1	-1	+1	2.218
3	11	-1	+1	-1	5.080
4	5	-1	+1	+1	2.218
5	13	+1	-1	-1	7.112
6	9	+1	-1	+1	3.105
7	6	+1	+1	-1	7.112
8	4	+1	+1	+1	3.105
9	19	0	-1	-1	6.096
10	14	0	-1	+1	2.662
11	21	0	+1	-1	6.096
12	16	0	+1	+1	2.662
13	8	-1	0	-1	5.080
14	15	+1	0	-1	7.112
15	10	-1	0	+1	2.218
16	18	+1	0	+1	3.105
17	17	-1	-1	0	3.088
18	12	-1	+1	0	3.088
19	20	+1	-1	0	4.323
20	3	+1	+1	0	4.323
21	1	0	0	0	3.705

Table 4: Experimental design matrix and corresponding energy density

3.5 MATERIAL SELECTION AND DETAIL

Specimens were fabricated on the Sinterstation® HiQ SLS® System located in the Engineering Teaching Center at the University of Texas at Austin. The work material was ALM PA 650 unfilled nylon 12 performance polyamide blend. The material had an average particle size of 55 μm [22]. A mixture of 30% fresh powder and 70% recycled powder was used to fabricate the test specimens.

3.6 DATA COLLECTION

3.6.1 Tensile properties

Tensile testing of ten specimens per experimental run was performed according to ASTM D638 [23] using Type I tensile bars. A clip-on extensometer was used to measure strain. The speed of testing was 5 mm/min. The average value for the tensile properties of interest and the standard deviations are shown in Tables 5-7.

Ex. #	Coded values			Actual values			Response: Ultimate tensile strength	
	X_1	X_2	X_3	Fill laser power, W	Outline laser power, W	Scan spacing, in	$\bar{Y}_1, MPa$	Std. Dev.
1	-1	-1	-1	20	3	0.006	43.0	0.41
2	-1	-1	+1	20	3	0.014	6.98	0.41
3	-1	+1	-1	20	7	0.006	40.6	1.24
4	-1	+1	+1	20	7	0.014	7.63	0.82
5	+1	-1	-1	28	3	0.006	44.5	0.62
6	+1	-1	+1	28	3	0.014	12.8	0.76
7	+1	+1	-1	28	7	0.006	46.1	0.87
8	+1	+1	+1	28	7	0.014	19.3	1.03
9	0	-1	-1	24	3	0.006	10.7	1.35
10	0	-1	+1	24	3	0.014	7.03	0.39
11	0	+1	-1	24	7	0.006	38.3	1.56
12	0	+1	+1	24	7	0.014	6.81	0.51
13	-1	0	-1	20	5	0.006	41.3	0.41
14	+1	0	-1	28	5	0.006	44.2	0.44
15	-1	0	+1	20	5	0.014	6.85	0.32
16	+1	0	+1	28	5	0.014	11.3	1.26
17	-1	-1	0	20	3	0.010	14.6	1.44
18	-1	+1	0	20	7	0.010	17.1	0.66
19	+1	-1	0	28	3	0.010	23.0	3.25
20	+1	+1	0	28	7	0.010	35.8	2.03
21	0	0	0	24	5	0.010	27.4	1.45
						$\bar{\bar{Y}}_1$ =	24.1	

Table 5: Average ultimate tensile strength and standard deviation

Ex. #	Coded values			Actual values			Response: Tensile modulus	
	X_1	X_2	X_3	Fill laser power, *W*	Outline laser power, *W*	Scan spacing, *in*	$\bar{Y}_2$, *MPa*	Std. Dev.
1	-1	-1	-1	20	3	0.006	1367	187
2	-1	-1	+1	20	3	0.014	308	43.6
3	-1	+1	-1	20	7	0.006	1504	160
4	-1	+1	+1	20	7	0.014	413	94.5
5	+1	-1	-1	28	3	0.006	1230	243
6	+1	-1	+1	28	3	0.014	715	260
7	+1	+1	-1	28	7	0.006	1320	152
8	+1	+1	+1	28	7	0.014	633	78.1
9	0	-1	-1	24	3	0.006	502	85.8
10	0	-1	+1	24	3	0.014	266	29.8
11	0	+1	-1	24	7	0.006	1120	238
12	0	+1	+1	24	7	0.014	407	75.8
13	-1	0	-1	20	5	0.006	1527	206
14	+1	0	-1	28	5	0.006	1280	170
15	-1	0	+1	20	5	0.014	359	40.4
16	+1	0	+1	28	5	0.014	443	61.6
17	-1	-1	0	20	3	0.010	687	108
18	-1	+1	0	20	7	0.010	917	138
19	+1	-1	0	28	3	0.010	666	94.6
20	+1	+1	0	28	7	0.010	1195	159
21	0	0	0	24	5	0.010	1095	243
						$\bar{\bar{Y}}_2$ =	855	

Table 6: Average tensile modulus and standard deviation

Ex. #	Coded values			Actual values			Response: Elongation-at-break	
	X_1	X_2	X_3	Fill laser power, *W*	Outline laser power, *W*	Scan spacing, *in*	$\bar{Y}_3$, *%*	Std. Dev.
1	-1	-1	-1	20	3	0.006	8.91	1.97
2	-1	-1	+1	20	3	0.014	1.68	0.60
3	-1	+1	-1	20	7	0.006	4.12	1.11
4	-1	+1	+1	20	7	0.014	2.64	0.85
5	+1	-1	-1	28	3	0.006	11.7	2.01
6	+1	-1	+1	28	3	0.014	0.94	0.33
7	+1	+1	-1	28	7	0.006	12.3	2.55
8	+1	+1	+1	28	7	0.014	3.12	1.19
9	0	-1	-1	24	3	0.006	2.70	0.56
10	0	-1	+1	24	3	0.014	1.91	0.82
11	0	+1	-1	24	7	0.006	4.37	1.24
12	0	+1	+1	24	7	0.014	1.14	0.54
13	-1	0	-1	20	5	0.006	6.92	1.83
14	+1	0	-1	28	5	0.006	11.1	2.04
15	-1	0	+1	20	5	0.014	1.23	0.41
16	+1	0	+1	28	5	0.014	2.35	0.73
17	-1	-1	0	20	3	0.010	1.12	0.58
18	-1	+1	0	20	7	0.010	1.39	0.48
19	+1	-1	0	28	3	0.010	1.39	0.52
20	+1	+1	0	28	7	0.010	2.78	0.69
21	0	0	0	24	5	0.010	1.74	0.54
							$\bar{\bar{Y}}_3$ =	4.07

Table 7: Average tensile elongation-at-break and standard deviation

3.6.2 Density property

Density testing of five specimens per experimental run was performed according to ASTM D792 Test Method A [24]. The temperature of the water was 22.5 °C. The average density and standard deviation for each experimental run is shown in Table 8.

Ex. #	Coded values			Actual values			Response: Density	
	X_1	X_2	X_3	Fill laser power, *W*	Outline laser power, *W*	Scan spacing, *in*	$\bar{Y}_4$, *g/cm³*	Std. Dev.
1	-1	-1	-1	20	3	0.006	0.981	0.008
2	-1	-1	+1	20	3	0.014	0.669	0.009
3	-1	+1	-1	20	7	0.006	0.990	0.010
4	-1	+1	+1	20	7	0.014	0.693	0.018
5	+1	-1	-1	28	3	0.006	0.959	0.022
6	+1	-1	+1	28	3	0.014	0.763	0.020
7	+1	+1	-1	28	7	0.006	0.991	0.004
8	+1	+1	+1	28	7	0.014	0.837	0.012
9	0	-1	-1	24	3	0.006	0.752	0.008
10	0	-1	+1	24	3	0.014	0.692	0.021
11	0	+1	-1	24	7	0.006	0.974	0.027
12	0	+1	+1	24	7	0.014	0.675	0.011
13	-1	0	-1	20	5	0.006	0.959	0.024
14	+1	0	-1	28	5	0.006	0.978	0.020
15	-1	0	+1	20	5	0.014	0.673	0.014
16	+1	0	+1	28	5	0.014	0.753	0.016
17	-1	-1	0	20	3	0.010	0.813	0.009
18	-1	+1	0	20	7	0.010	0.835	0.012
19	+1	-1	0	28	3	0.010	0.944	0.022
20	+1	+1	0	28	7	0.010	0.944	0.019
21	0	0	0	24	5	0.010	0.934	0.007
							$\bar{\bar{Y}}_4$ = 0.848	

Table 8: Average density and standard deviation

3.6.3 Hardness property

Hardness testing of 2 specimens per experimental run was performed according to ASTM D2240 [25]. The ambient air temperature was 72.0 °F. The tests were performed using a hand-held XF Shore-D durometer. The test specimens were 1” cubes. The average hardness and standard deviation for each experimental run is shown in Table 9.

Ex. #	Coded values			Actual values			Response: Hardness	
	X_1	X_2	X_3	Fill laser power, *W*	Outline laser power, *W*	Scan spacing, *in*	$\bar{Y}_5$	Std. Dev.
1	-1	-1	-1	20	3	0.006	74.7	0.15
2	-1	-1	+1	20	3	0.014	58.2	2.05
3	-1	+1	-1	20	7	0.006	73.4	0.75
4	-1	+1	+1	20	7	0.014	59.1	3.90
5	+1	-1	-1	28	3	0.006	73.4	1.00
6	+1	-1	+1	28	3	0.014	62.5	0.35
7	+1	+1	-1	28	7	0.006	74.2	1.15
8	+1	+1	+1	28	7	0.014	66.3	2.10
9	0	-1	-1	24	3	0.006	58.8	1.85
10	0	-1	+1	24	3	0.014	58.3	0.70
11	0	+1	-1	24	7	0.006	71.7	1.70
12	0	+1	+1	24	7	0.014	57.8	0.35
13	-1	0	-1	20	5	0.006	73.9	0.10
14	+1	0	-1	28	5	0.006	74.4	0.10
15	-1	0	+1	20	5	0.014	56.9	0.65
16	+1	0	+1	28	5	0.014	60.0	0.60
17	-1	-1	0	20	3	0.010	65.4	0.20
18	-1	+1	0	20	7	0.010	64.8	0.61
19	+1	-1	0	28	3	0.010	67.5	1.80
20	+1	+1	0	28	7	0.010	71.4	0.20
21	0	0	0	24	5	0.010	70.5	1.15
							$\bar{\bar{Y}}_5$ =	66.3

Table 9: Average hardness and standard deviation

3.6.4 Surface roughness property

Surface roughness of 2 specimens per experimental run was performed with roughness measurements obtained using a Wyko NT 9100 Optical Profilometer. Specimens were gold-sputtered prior to analysis to reduce the reflectivity of the white nylon specimens and to ensure that an accurate reading of the surface could be achieved. The average surface roughness and standard deviation for each experimental run is shown in Table 10.

Ex. #	Coded values			Actual values			Response: Surface roughness	
	X_1	X_2	X_3	Fill laser power, *W*	Outline laser power, *W*	Scan spacing, *in*	$\bar{Y}_6, \mu m$	Std. Dev.
1	-1	-1	-1	20	3	0.006	17.51	1.025
2	-1	-1	+1	20	3	0.014	19.76	0.460
3	-1	+1	-1	20	7	0.006	18.06	0.675
4	-1	+1	+1	20	7	0.014	30.95	0.940
5	+1	-1	-1	28	3	0.006	17.34	1.860
6	+1	-1	+1	28	3	0.014	18.48	0.110
7	+1	+1	-1	28	7	0.006	15.46	1.270
8	+1	+1	+1	28	7	0.014	21.45	1.615
9	0	-1	-1	24	3	0.006	27.90	2.000
10	0	-1	+1	24	3	0.014	24.50	2.535
11	0	+1	-1	24	7	0.006	17.65	0.160
12	0	+1	+1	24	7	0.014	26.35	0.785
13	-1	0	-1	20	5	0.006	15.65	0.475
14	+1	0	-1	28	5	0.006	26.05	0.140
15	-1	0	+1	20	5	0.014	26.69	3.435
16	+1	0	+1	28	5	0.014	25.65	0.065
17	-1	-1	0	20	3	0.010	23.52	0.765
18	-1	+1	0	20	7	0.010	24.94	1.380
19	+1	-1	0	28	3	0.010	24.73	2.895
20	+1	+1	0	28	7	0.010	21.85	0.035
21	0	0	0	24	5	0.010	24.67	0.030
							$\bar{\bar{Y}}_6$ =	28.34

Table 10: Average surface roughness and standard deviation

Chapter 4: Results and Discussion

4.1 EXPERIMENTAL RESULTS

Table 11 summarizes the experimental data gathered from all test specimens for each experimental run. The models and optimization are based on the presented data.

Ex #	Actual values			Response variables					
	Fill laser power X_1, W	Outline laser power X_2, W	Scan spacing X_3, in	Tensile Strength Y_1, MPa	Tensile Modulus Y_2, MPa	Elongation-at-break $Y_3, \%$	Density $Y_4, g/cm^3$	Hardness Y_5	Surface roughness $Y_6, \mu m$
1	20	3	0.006	43.0	1367	8.91	0.981	74.7	17.51
2	20	3	0.014	6.98	308	1.68	0.669	58.2	19.76
3	20	7	0.006	40.6	1504	4.12	0.990	73.4	18.06
4	20	7	0.014	7.63	413	2.64	0.693	59.1	30.95
5	28	3	0.006	44.5	1230	11.7	0.959	73.4	17.34
6	28	3	0.014	12.8	715	0.94	0.763	62.5	18.48
7	28	7	0.006	46.1	1320	12.3	0.991	74.2	15.46
8	28	7	0.014	19.3	633	3.12	0.837	66.3	21.45
9	24	3	0.006	10.7	502	2.70	0.752	58.8	27.90
10	24	3	0.014	7.03	266	1.91	0.692	58.3	24.50
11	24	7	0.006	38.3	1120	4.37	0.974	71.7	17.65
12	24	7	0.014	6.81	407	1.14	0.675	57.8	26.35
13	20	5	0.006	41.3	1527	6.92	0.959	73.9	15.65
14	28	5	0.006	44.2	1280	11.1	0.978	74.4	26.05
15	20	5	0.014	6.85	359	1.23	0.673	56.9	26.69
16	28	5	0.014	11.3	443	2.35	0.753	60.0	25.65
17	20	3	0.010	14.6	687	1.12	0.813	65.4	23.52
18	20	7	0.010	17.1	917	1.39	0.835	64.8	24.94
19	28	3	0.010	23.0	666	1.39	0.944	67.5	24.73
20	28	7	0.010	35.8	1195	2.78	0.944	71.4	21.85
21	24	5	0.010	27.4	1095	1.74	0.934	70.5	24.67

Table 11: Experimental design and average collected data

4.2 MODELS FOR MECHANICAL PROPERTIES

Quadratic models are obtained for all response variables based on the data shown in Table 11 and using least-squares fitting implemented via Minitab [27]. The models represent an empirical relationship between the process variables and the measured responses, with the quadratic form providing terms for main effects, squared terms, interaction effects and error.

The models are refined using backwards elimination to remove insignificant factors outside of an alpha level of 0.10 [28], leaving only model terms that significantly affect the response variable of interest, with significance established with 90% confidence.

The process parameters are represented in the models as the following: fill laser power (A), outline laser power (B), and scan spacing (C).

Ultimate tensile strength

The quadratic model for ultimate tensile strength is given in Equation 3:

$$Y_1 = 3.270\ x\ 10^2 - 24.2\ A + 4.60\ B - 5.179\ x\ 10^3\ C + 0.489\ A^2 - 0.598\ B^2 + 5.593\ x\ 10^4\ C^2 + 0.209\ AB + 62.0\ AC - 2.050\ x\ 10^2\ BC \quad (3)$$

Insignificant model terms were removed from Equation 3 with backwards elimination to improve the models. The reduced model for ultimate tensile strength, given in Equation 4, includes fill laser power and its square term, and scan spacing as significant effects.

$$Y_1 = 3.08\ x\ 10^2 - 22.8\ A + 1.530\ B - 3.539\ x\ 10^3\ C + 0.494\ A^2 \quad (4)$$

Figure 2 graphs the contour plots of the reduced model for ultimate tensile strength. Figure 3 shows the curvature for each of the surface plots of the reduced model for ultimate tensile strength. Based on the model (4), the optimal parameter settings to maximize tensile strength are setting fill laser power at 28 W, outline laser power at 7 W, and scan spacing at 0.006 in.

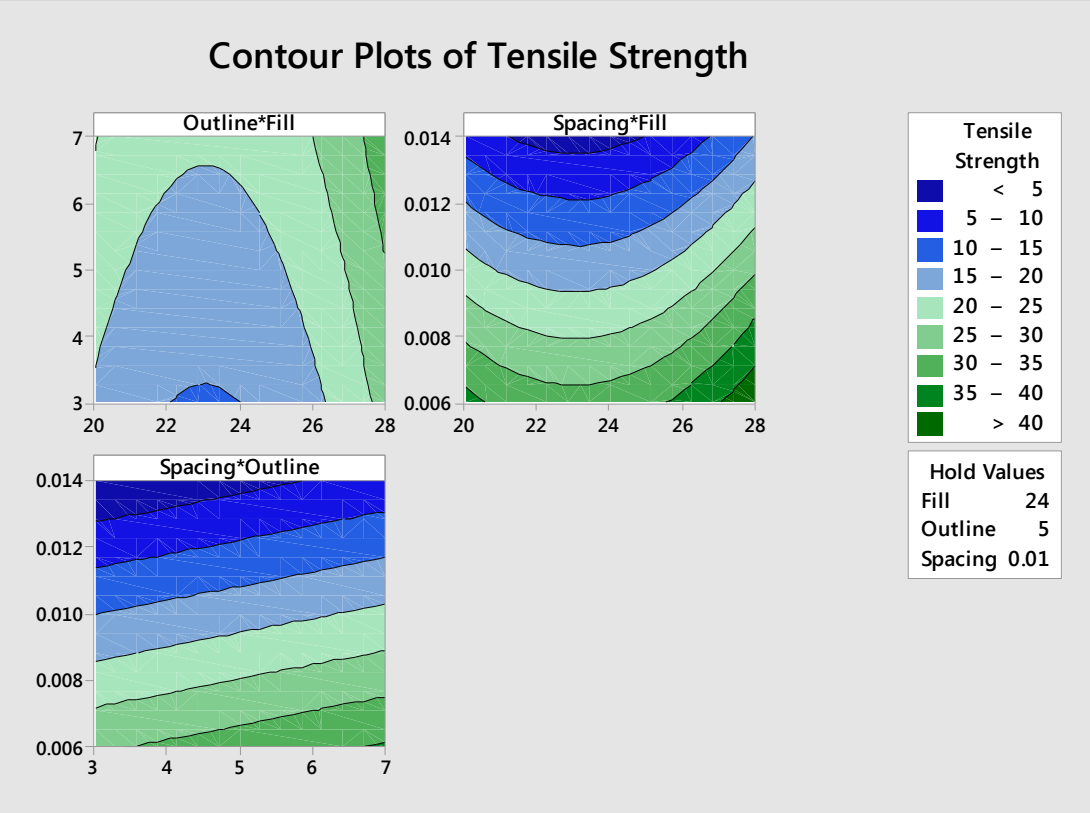

Figure 2: Contour plots of reduced model for ultimate tensile strength

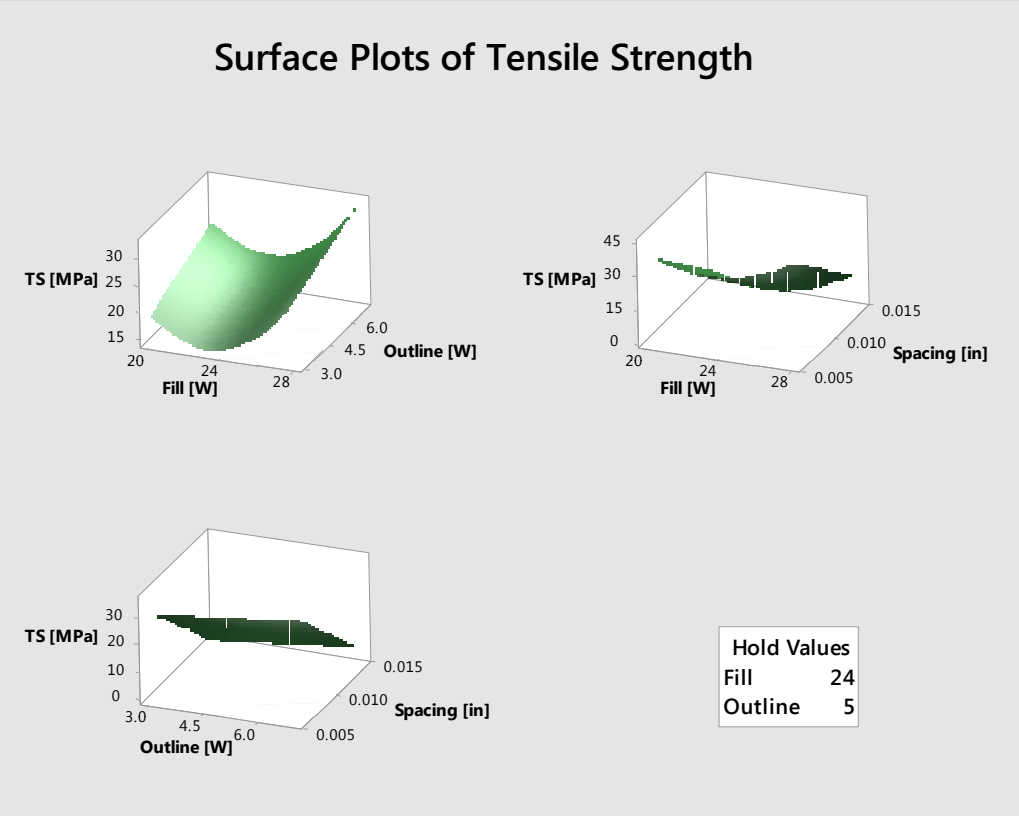

Figure 3: Surface plots of reduced model for ultimate tensile strength

Tensile modulus

The full quadratic model for tensile modulus is given in Equation 5:

$$Y_2 = 9.666\ x\ 10^3 - 7.350\ x\ 10^2\ A + 3.720\ x\ 10^2 B - 1.367\ x\ 10^5\ C + 13.98\ A^2 - 26.2\ B^2 - 4.314\ x\ 10^6\ C^2 + 0.67\ AB + 6.663\ x\ 10^3\ AC - 7.091\ x\ 10^3 BC \quad (5)$$

After removing insignificant terms via backwards elimination, the reduced model for tensile modulus, given in Equation 6, includes fill laser power and its square term, outline laser power, scan spacing, and the interaction of fill laser power and scan spacing as significant effects.

$$Y_2 = 1.120\ x\ 10^4 - 7.570\ x\ 10^2\ A + 55.3B - 2.584\ x\ 10^5\ C + 14.52\ A^2 + 6.663\ x\ 10^3\ AC \quad (6)$$

Figure 4 graphs the contour plots of the reduced model for tensile modulus. Figure 5 shows the curvature for each of the surface plots of the reduced model for tensile modulus. Following model (6), the optimal parameter settings in order to maximize tensile modulus are setting fill laser power at 20 W, outline laser power at 7 W, and scan spacing at 0.006 in.

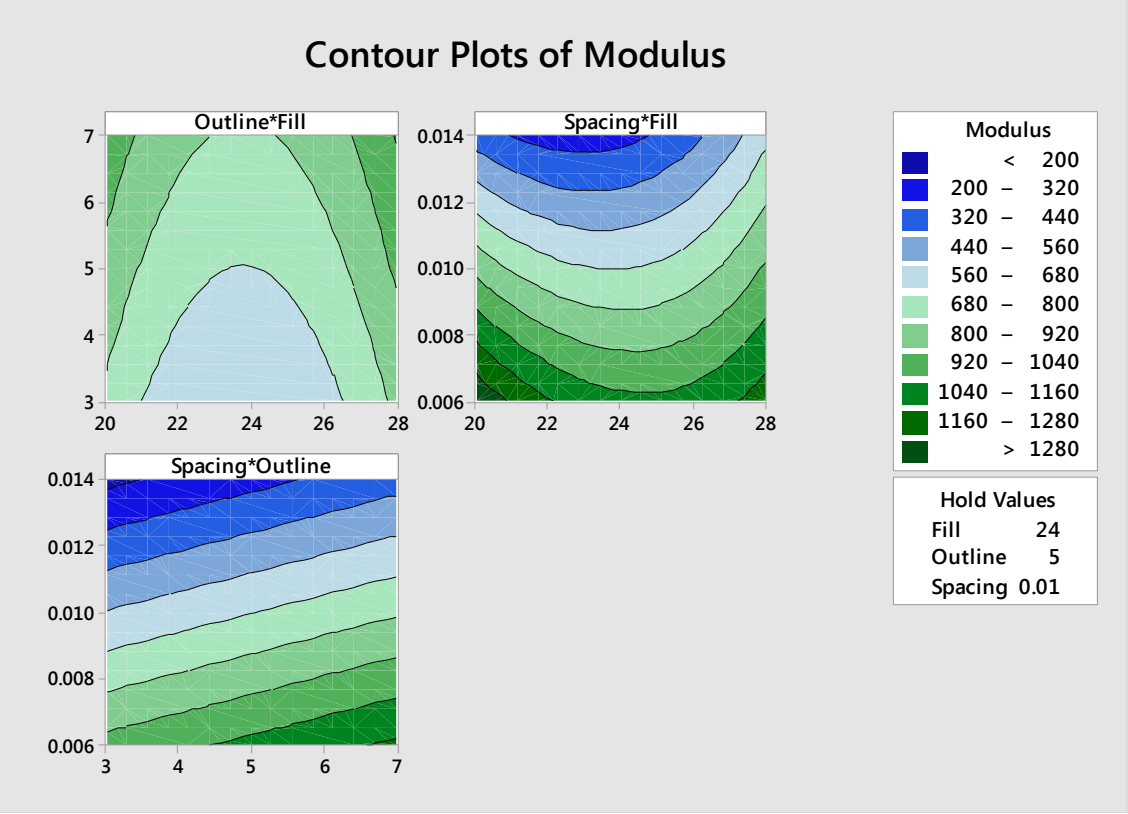

Figure 4: Contour plots of reduced model for tensile modulus

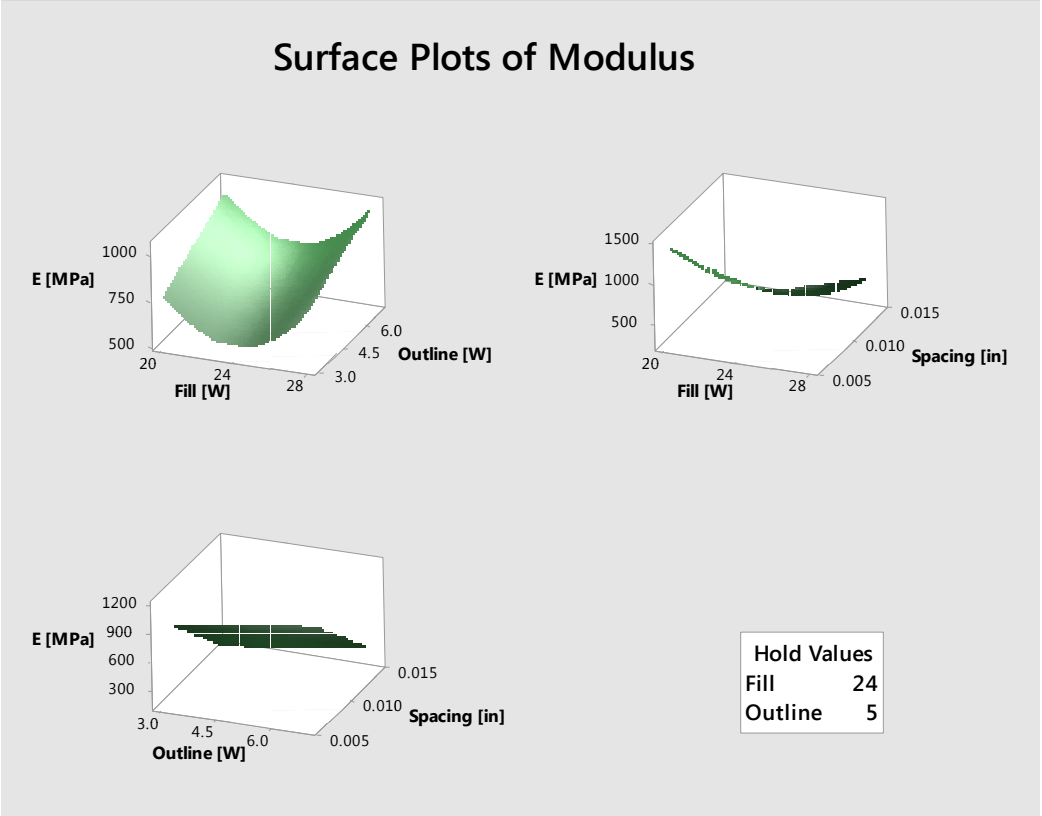

Figure 5: Surface plots of reduced model for tensile modulus

Elongation-at-break

The full quadratic model for elongation-at-break is given in Equation 7:

$$Y_3 = 97.3 - 6.48\,A - 1.16\,B - 3.243\,x\,10^3\,C + 0.1478\,A^2 - 0.124\,B^2 + 2.016\,x\,10^5\,C^2 + 0.0808\,AB - 74.0\,AC + 50.7\,BC \quad (7)$$

After removing insignificant terms via backwards elimination, the simplified elongation-at-break model, given in Equation 8, includes fill laser power and its square term, scan spacing and its square term, and the interaction between fill laser power and scan spacing as significant effects.

$$Y_3 = 89.1 - 6.16\,A - 3.022\,x\,10^3\,C + 0.1494\,A^2 + 2.032\,x\,10^5\,C^2 - 74.0\,AC \quad (8)$$

Figure 6 graphs the contour plot of the reduced model for elongation-at-break. Figure 7 shows the curvature for the surface plot of the reduced model for elongation-at-break. Following model (8), the optimal parameter settings in order to maximize elongation-at-break are setting fill laser power at 28 W, outline laser power at 7 W, and scan spacing at 0.006 in.

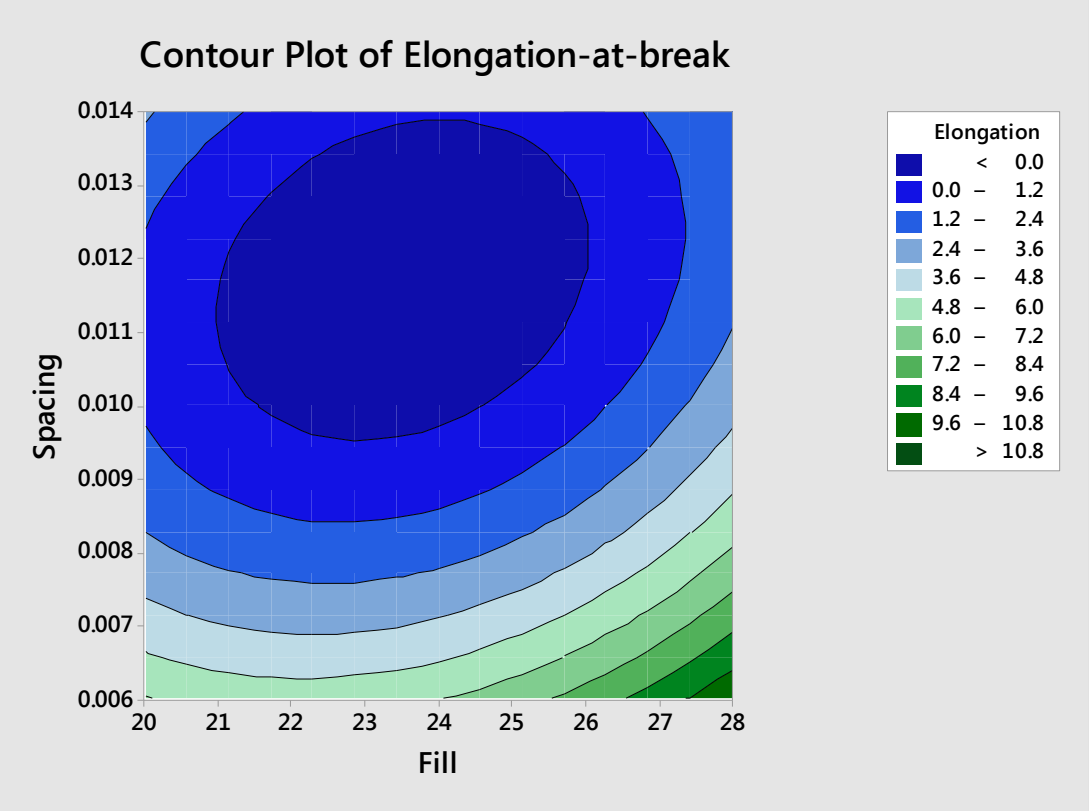

Figure 6: Contour plot of reduced model for elongation-at-break

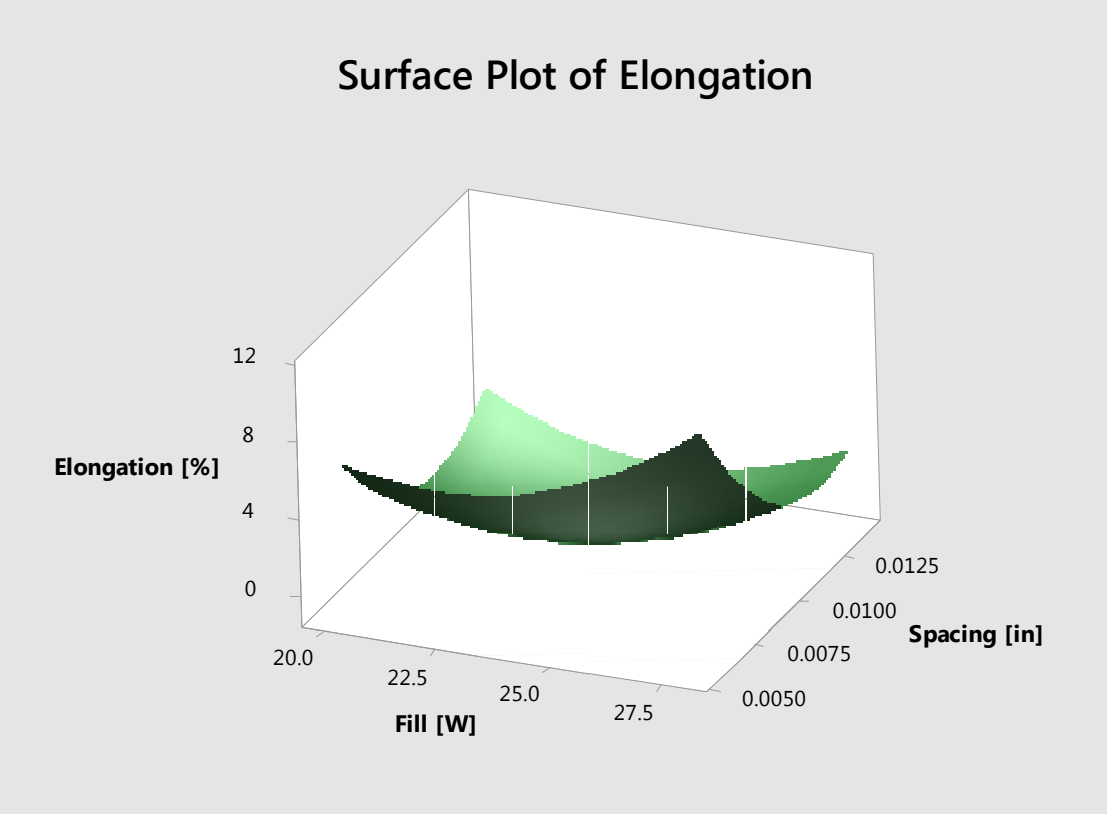

Figure 7: Surface plot of reduced model for elongation-at-break

Sintered part density

The full quadratic model for density is given in Equation 9:

$$Y_4 = 2.67 - 0.1674\,A + 0.0557\,B + 13.9\,C + 0.00327\,A^2 - 0.00382\,B^2 - 3.638\,x\,10^3\,C^2 + 0.00054\,AB + 1.66\,AC - 1.90\,BC \quad (9)$$

After removing insignificant terms via backwards elimination, the density model reduces to Equation 10 and includes fill laser power, scan spacing and its square term as significant effects.

$$Y_4 = 0.596 + 0.00866\,A + 46.5\,C - 3.753\,x\,10^3\,C^2 \quad (10)$$

Figure 8 graphs the contour plot of the reduced model for density. Figure 9 shows the curvature for the surface plot of the reduced model for density. Following model (10),

the optimal parameter settings in order to maximize density are setting fill laser power at 28 W, outline laser power at 7 W, and scan spacing at 0.007 in.

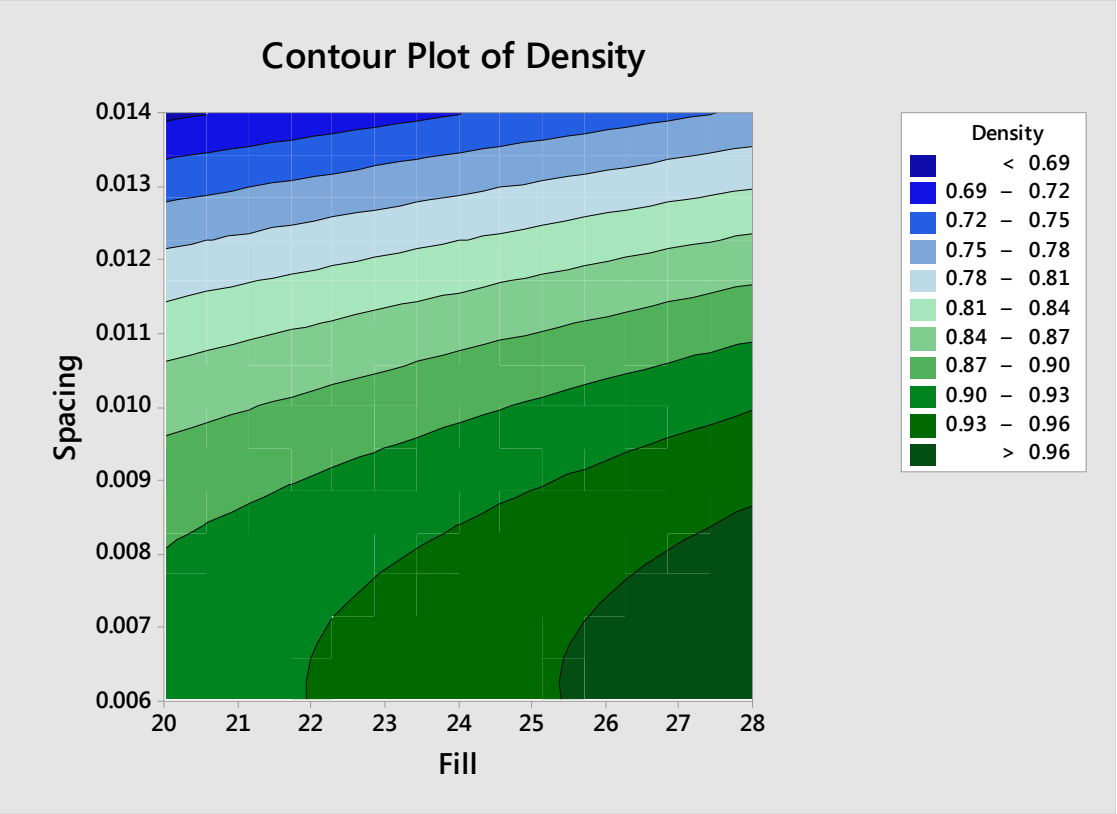

Figure 8: Contour plot of reduced model for density

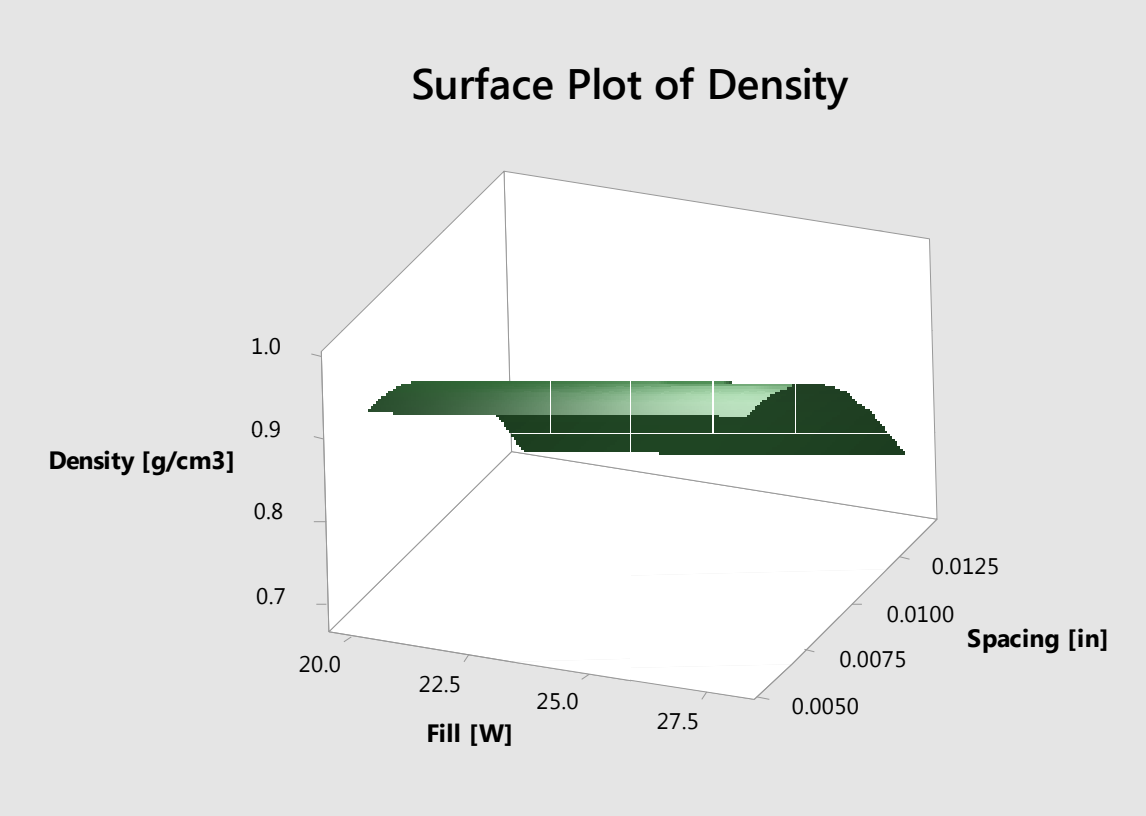

Figure 9: Surface plot of reduced model for density

Hardness

The full quadratic model for hardness is given in Equation 11:

$$Y_5 = 2.095\ x\ 10^2 - 11.97A + 1.50B - 4.72\ x\ 10^2\ C + 0.231\ A^2 - 0.240\ B^2 + 1.208\ x\ 10^5\ C^2 + 0.099\ AB + 76.0\ AC - 85\ BC \quad (11)$$

After removing insignificant terms via backwards elimination, the reduced hardness model, given in Equation 12, includes fill laser power and its square term, and scan spacing as significant effects.

$$Y_5 = 2.077\ x\ 10^2 - 11.14\ A - 1.491\ x\ 10^3\ C + 0.240\ A^2 \quad (12)$$

Figure 10 graphs the contour plot of the reduced model for hardness. Figure 11 shows the curvature for the surface plot of the reduced model for hardness. Following

model (12), the optimal parameter settings in order to maximize hardness are setting fill laser power at 28 W, outline laser power at 7 W, and scan spacing at 0.006 in.

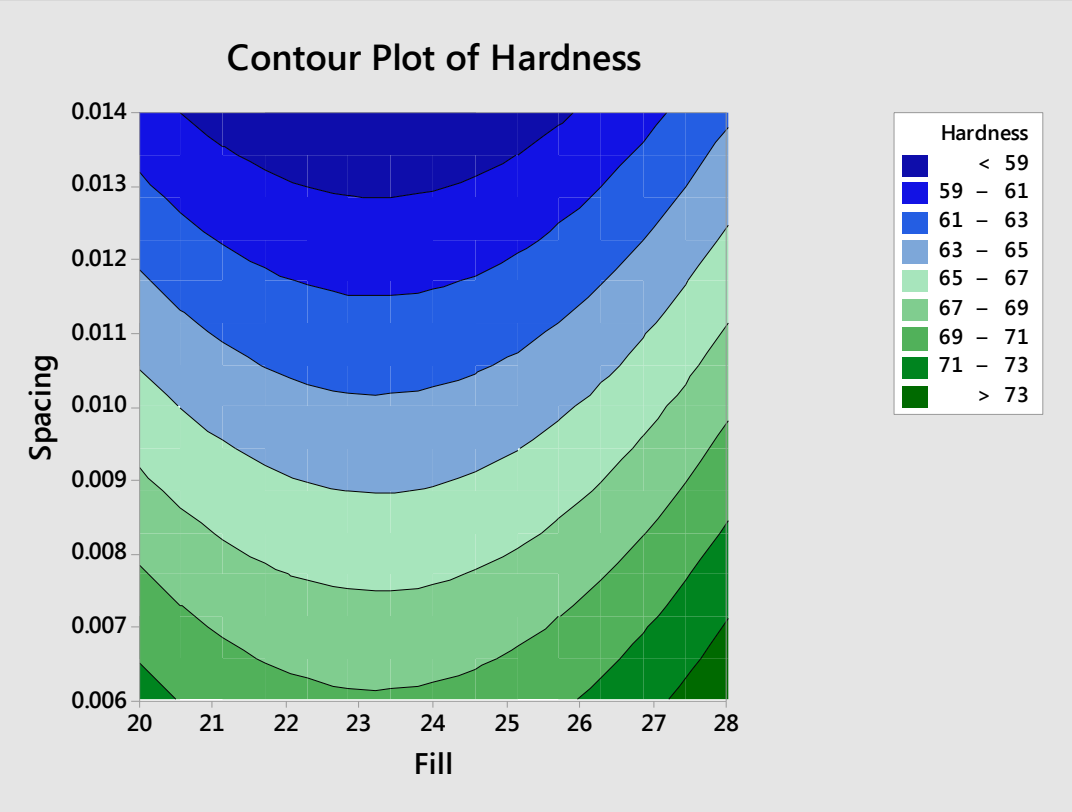

Figure 10: Contour plot of reduced model for hardness

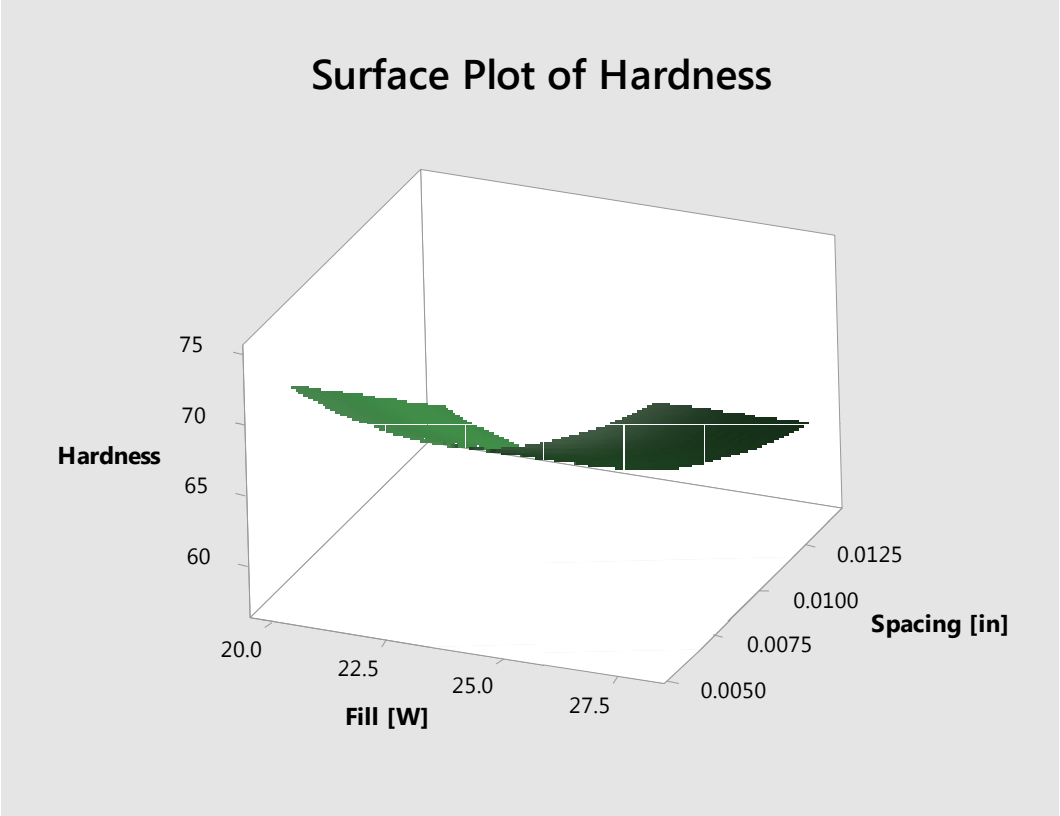

Figure 11: Surface plot of reduced model for hardness

Surface roughness

The full quadratic model for surface roughness is given in Equation 13:

$$Y_6 = -129.3 + 9.74\,A + 6.18\,B + 4.518x10^3\,C - 0.168\,A^2 - 0.522\,B^2 - 1.462x10^5\,C^2 - 0.156\,AB - 1.014x10^2\,AC + 2.87\,x\,10^2\,BC \quad (13)$$

After removing insignificant terms via backwards elimination, the reduced surface roughness model, given in Equation 14, includes outline laser power, scan spacing and their interaction as significant effects.

$$Y_6 = 30.27 - 2.78\,B - 8.40x10^2\,C + 2.87x10^2\,BC \quad (14)$$

Figure 12 graphs the contour plot of the reduced model for surface roughness. Figure 13 shows the curvature for the surface plot of the reduced model for surface

roughness. Following model (14), the optimal parameter settings in order to minimize surface roughness are setting fill laser power at 28 W, outline laser power at 7 W, and scan spacing at 0.006 in.

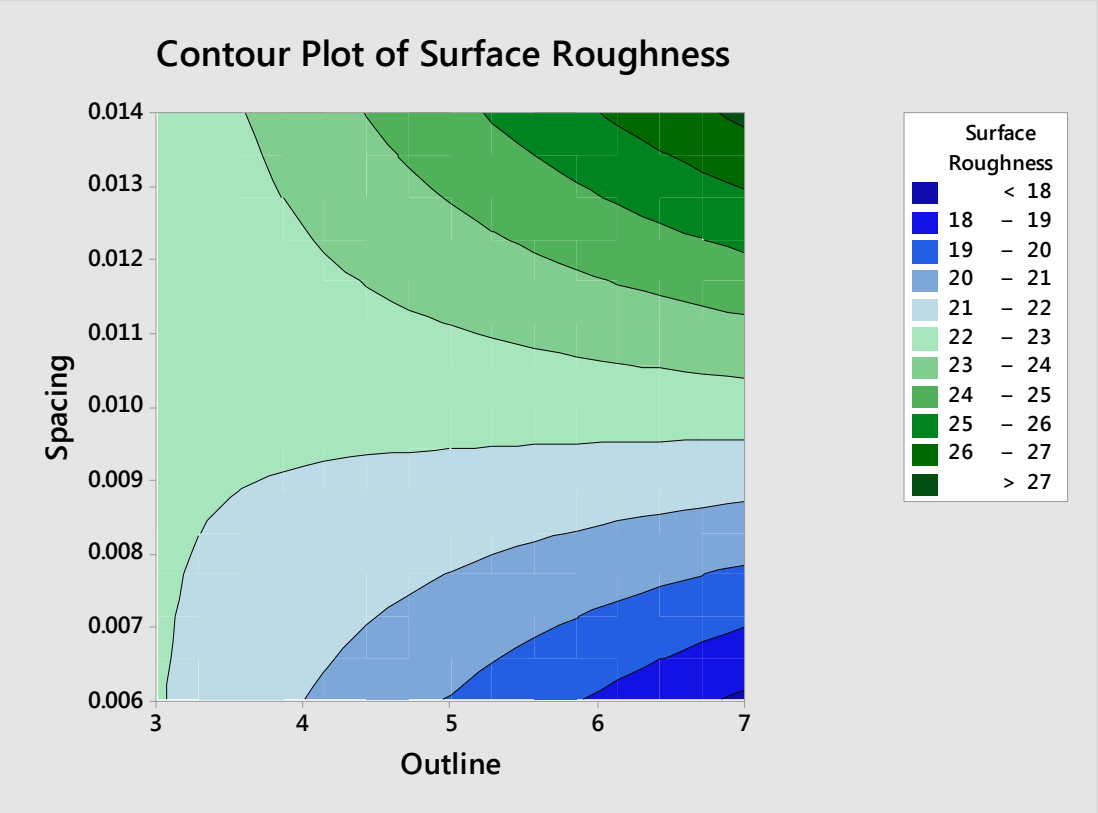

Figure 12: Contour plot of reduced model for surface roughness

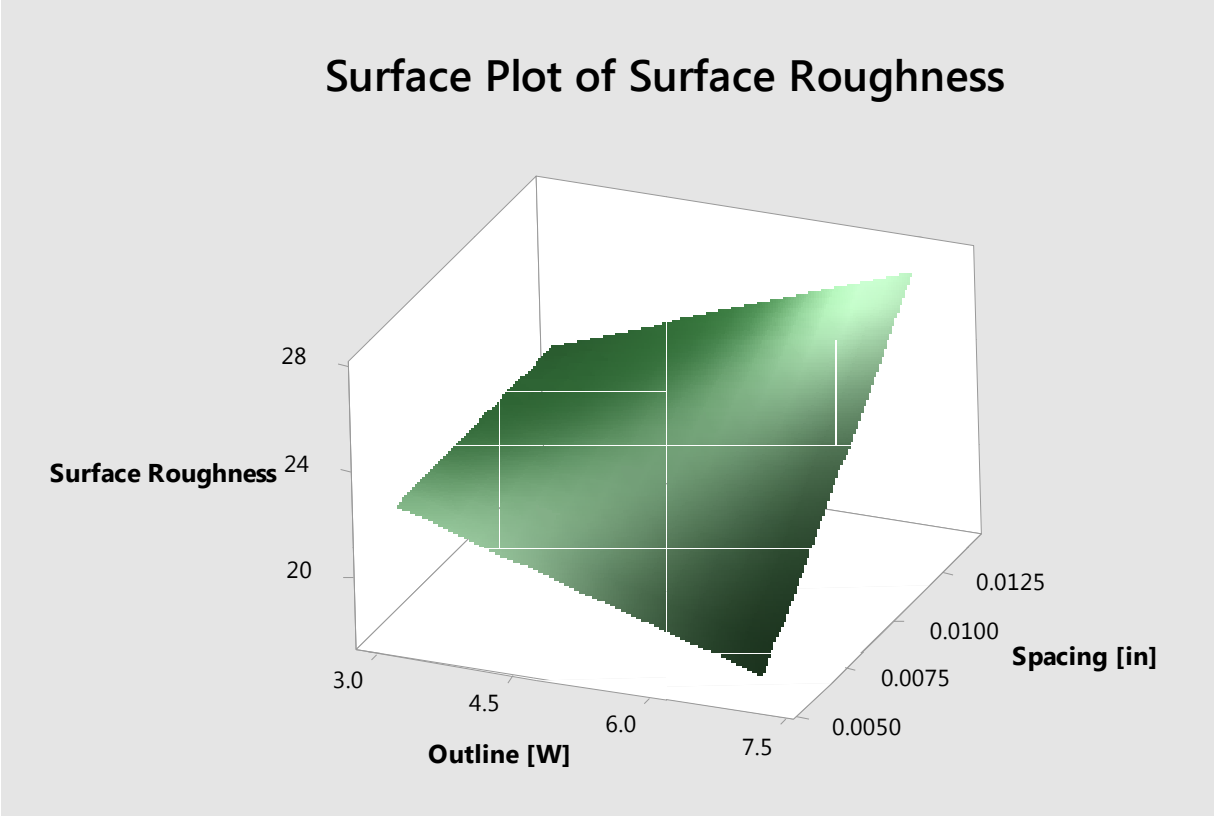

Figure 13: Surface plot of reduced model for surface roughness

4.3 ANOVA

ANOVA is performed on the collected data from Table 11 using Minitab [27]. Table 12 shows the ANOVA table for the full quadratic response models while Table 13 shows the ANOVA table for the reduced response models.

In Table 12, model F-value greater than 4.6375 and low probability value ($P < 0.5$) indicate that the model terms are significant. Model terms with P-value greater than 0.100 indicate insignificant model terms. The adjusted determination coefficient (Adj R^2) measures the percentage of variation explained by the independent variables. The predicted determination coefficient (Pred R^2) measures how well the model predicts responses for new observations. The Pred R^2 value should be within 0.20 of the Adj R^2 value, and a large

difference may indicate over-fitting of the model [29]. The adequate precision ratio (Adeq Precision) measures the signal-to-noise ratio. A ratio greater than 4 is desirable [30].

Ultimate tensile strength

In the full quadratic model, given by Equation 3, the value of the adjusted determination coefficient (Adj R^2 = 0.7470) indicates that the model explains 74.70% of the variability in the response. The Pred R^2 of 0.4915 is not in reasonable agreement with the Adj R^2 of 0.7470. The "Adeq Precision" ratio of 7.407 indicates an adequate signal.

In the reduced model, given by Equation 4, the value of the adjusted determination coefficient (Adj R^2 = 0.7783) indicates that the model explains 79.83% of the variability in the response. The Pred R^2 of 0.6902 is in reasonable agreement with the Adj R^2 of 0.7783. The "Adeq Precision" ratio of 11.73 indicates an adequate signal for the model.

Tensile modulus

In the full quadratic model, given by Equation 5, the value of the adjusted determination coefficient (Adj R^2 = 0.7468) indicates that the model explains 74.68% of the variability in the response. The Pred R^2 of 0.4794 is not in reasonable agreement with the Adj R^2 of 0.7468. The "Adeq Precision" ratio of 8.516 indicates an adequate signal.

In the reduced model, given by Equation 6, the value of the adjusted determination coefficient (Adj R^2 = 0.7791) indicates that the model explains 77.91% of the variability in the response. The Pred R^2 of 0.6825 is in reasonable agreement with the Adj R^2 of 0.7791. The "Adeq Precision" ratio of 11.77 indicates an adequate signal for the model.

Elongation-at-break

In the full quadratic model, given by Equation 7, the value of the adjusted determination coefficient (Adj R^2 = 0.7474) indicates that the model explains 74.74% of

the variability in the response. The Pred R^2 of 0.4990 is not in reasonable agreement with the Adj R^2 of 0.7474. The "Adeq Precision" ratio of 8.820 indicates an adequate signal.

In the reduced model, given by Equation 8, the value of the adjusted determination coefficient (Adj R^2 = 0.7764) indicates that the model explains 77.64% of the variability in the response. The Pred R^2 of 0.6683 is in reasonable agreement with the Adj R^2 of 0.7764. The "Adeq Precision" ratio of 12.10 indicates an adequate signal for the model.

Sintered part density

In the full quadratic model, given by Equation 9, the value of the adjusted determination coefficient (Adj R^2 = 0.7891) indicates that the model explains 78.91% of the variability in the response. The Pred R^2 of 0.5720 is not in reasonable agreement with the Adj R^2 of 0.7891. The "Adeq Precision" ratio of 8.149 indicates an adequate signal.

In the reduced model, given by Equation 10, the value of the adjusted determination coefficient (Adj R^2 = 0.7438) indicates that the model explains 74.38% of the variability in the response. The Pred R^2 of 0.6948 is in reasonable agreement with the Adj R^2 of 0.7438. The "Adeq Precision" ratio of 11.73 indicates an adequate signal for the model.

Hardness

In the full quadratic model, given by Equation 11, the value of the adjusted determination coefficient (Adj R^2 = 0.6813) indicates that the model explains 68.13% of the variability in the response. The Pred R^2 of 0.3548 is not in reasonable agreement with the Adj R^2 of 0.6813. The "Adeq Precision" ratio of 2.645 does not indicate an adequate signal.

In the reduced model, given by Equation 12, the value of the adjusted determination coefficient (Adj R^2 = 0.6975) indicates that the model explains 69.75% of the variability

in the response. The Pred R^2 of 0.5670 is in reasonable agreement with the Adj R^2 of 0.6975. The "Adeq Precision" ratio of 6.969 indicates an adequate signal for the model.

Surface roughness

In the full quadratic model, given by Equation 13, the value of the adjusted determination coefficient (Adj R^2 = 0.4162) indicates that the model explains 41.62% of the variability in the response. The Pred R^2 of 0.00 is not in reasonable agreement with the Adj R^2 of 0.4162. The "Adeq Precision" ratio of 2.843 does not indicate an adequate signal.

In the reduced model, given by Equation 14, the value of the adjusted determination coefficient (Adj R^2 = 0. 0.2892) indicates that the model explains 28.92% of the variability in the response. The Pred R^2 of 0.0226 is not in reasonable agreement with the Adj R^2 of 0.2892. The "Adeq Precision" ratio of 5.836 indicates an adequate signal for the model.

Source	Sum of squares	DF	Mean square	F value	P-value	$F > F_{crit}$
Ultimate tensile strength						
Model	4,012.74	9	445.86	7.56	0.001	*Significant*
A	217.67	1	217.67	3.69	0.081	
B	149.78	1	149.78	2.54	0.139	
C	3304.24	1	3,304.24	56.04	0.000	
A^2	231.87	1	231.87	3.93	0.073	
B^2	21.70	1	21.70	0.37	0.556	
C^2	3.03	1	3.03	0.05	0.825	
AB	33.51	1	33.51	0.57	0.467	
AC	11.91	1	11.91	0.20	0.662	
BC	32.40	1	32.40	0.55	0.474	
Error	648.61	11	58.96			
Total	4,661.35	20				
Std. Dev.			7.6788	R-Squared	0.8609	
Mean			24.057	Adj R-Squared	0.7470	
C.V.			31.92	Pred R-Squared	0.4915	
PRESS			2,370.37	Adeq Precision	7.407	
Tensile modulus						
Model	3,128,353	9	347,595	7.55	0.001	*Significant*
A	9,996	1	9,996	0.22	0.650	
B	195,715	1	195,715	4.25	0.064	
C	2,484,613	1	2,484,613	53.99	0.000	
A^2	205,701	1	189,595	4.12	0.067	
B^2	38,921	1	41,649	0.90	0.362	
C^2	18,057	1	18,057	0.39	0.544	
AB	342	1	342	0.01	0.933	
AC	136,393	1	136,393	2.96	0.113	
BC	38,617	1	38,617	0.84	0.379	
Error	506,254	11	46,023			
Total	3,634,608	20				
Std. Dev.			214.530	R-Squared	0.8607	
Mean			855.038	Adj R-Squared	0.7468	
C.V.			25.09	Pred R-Squared	0.4794	
PRESS			1,892,210	Adeq Precision	8.516	

Table 12: ANOVA table of statistical results for quadratic response models

Source	Sum of squares	DF	Mean square	F value	P-value	$F > F_{crit}$
Elongation-at-break						
Model	241.494	9	26.833	7.58	0.001	*Significant*
A	19.307	1	19.307	5.45	0.040	
B	0.149	1	0.149	0.04	0.841	
C	138.204	1	138.204	39.02	0.000	
A^2	18.905	1	21.180	5.98	0.014	
B^2	1.683	1	0.932	0.26	0.618	
C^2	39.417	1	39.417	11.13	0.007	
AB	5.013	1	5.013	1.32	0.259	
AC	16.841	1	16.841	4.75	0.052	
BC	1.975	1	1.975	0.56	0.471	
Error	38.961	11	3.542			
Total	280.455	20				
Std. Dev.			1.882	R-Squared	0.8611	
Mean			4.070	Adj R-Squared	0.7474	
C.V.			46.24	Pred R-Squared	0.4990	
PRESS			140.503	Adeq Precision	8.820	
Density						
Model	0.272929	9	0.030325	9.32	0.001	*Significant*
A	0.019218	1	0.019218	5.90	0.033	
B	0.008382	1	0.008382	2.57	0.137	
C	0.208541	1	0.208541	64.06	0.000	
A^2	0.011923	1	0.010353	3.18	0.102	
B^2	0.000568	1	0.000885	0.27	0.612	
C^2	0.012838	1	0.012838	3.94	0.073	
AB	0.000225	1	0.000225	0.07	0.797	
AC	0.008456	1	0.008456	2.60	0.135	
BC	0.002778	1	0.002778	0.85	0.375	
Error	0.035809	11	0.003255			
Total	0.308738	20				
Std. Dev.			0.057	R-Squared	0.8840	
Mean			0.848	Adj R-Squared	0.7891	
C.V.			6.728	Pred R-Squared	0.5720	
PRESS			0.132138	Adeq Precision	8.179	

Table 12 (cont.): ANOVA table of statistical results for quadratic response models

Source	Sum of squares	DF	Mean square	F value	P-value	$F > F_{crit}$
Hardness						
Model	731.408	9	81.268	5.75	0.004	*Significant*
A	33.931	1	33.931	2.40	0.150	
B	24.751	1	24.751	1.75	0.213	
C	568.823	1	568.823	40.25	0.000	
A^2	56.064	1	51.644	3.65	0.082	
B^2	2.788	1	3.480	0.25	0.629	
C^2	14.164	1	14.164	1.00	0.338	
AB	7.521	1	7.521	0.53	0.481	
AC	17.763	1	17.763	1.26	0.286	
BC	5.603	1	5.603	0.40	0.542	
Error	155.464	11	14.133			
Total	886.871	20				
Std. Dev.			3.76	R-Squared	0.8247	
Mean			66.3	Adj R-Squared	0.6813	
C.V.			5.67	Pred R-Squared	0.3548	
PRESS			572.238	Adeq Precision	2.645	
Surface roughness						
Model	266.172	9	29.5747	2.58	0.070	
A	2.299	1	2.2990	0.20	0.663	
B	0.551	1	0.5513	0.05	0.830	
C	91.203	1	91.2025	7.97	0.017	
A^2	23.038	1	27.2302	2.38	0.151	
B^2	14.691	1	16.5429	1.45	0.254	
C^2	20.739	1	20.7386	1.81	0.205	
AB	18.650	1	18.6501	1.63	0.228	
AC	31.590	1	31.5901	2.76	0.125	
BC	63.411	1	63.4110	5.54	0.038	
Error	125.875	11	11.4432			
Total	392.048	20				
Std. Dev.			3.38278	R-Squared	0.6789	
Mean			22.3383	Adj R-Squared	0.4162	
C.V.			15.1434	Pred R-Squared	0.0000	
PRESS			475.014	Adeq Precision	2.843	

Table 12 (cont.): ANOVA table of statistical results for quadratic response models

Source	Sum of squares	DF	Mean square	F value	P-value	$F > F_{crit}$
Ultimate tensile strength						
Model	3,909.3	4	977.32	20.79	0.000	Significant
A	217.7	1	217.67	4.63	0.047	
B	149.8	1	149.78	3.19	0.093	
C	3,304.2	1	3,304.24	70.30	0.000	
A^2	237.6	1	237.58	5.05	0.039	
Error	901.9	16	47.01			
Total	4,661.3	20				
Std. Dev.			6.85603	R-Squared	0.8387	
Mean			24.057	Adj R-Squared	0.7983	
C.V.			27.25	Pred R-Squared	0.6902	
PRESS			1,444.23	Adeq Precision	11.73	
Tensile modulus						
Model	3,032,417	5	606,483	15.11	0.000	Significant
A	9,996	1	9,996	0.25	0.625	
B	195,715	1	195,715	4.88	0.043	
C	2,484,613	1	2,484,613	61.89	0.000	
A^2	205,701	1	205,701	5.12	0.039	
AC	136,393	1	136,393	3.40	0.085	
Error	602,190	15	40,146			
Total	3,634,608	20				
Std. Dev.			200.365	R-Squared	0.8343	
Mean			855.038	Adj R-Squared	0.7791	
C.V.			23.43	Pred R-Squared	0.6825	
PRESS			1,153,813	Adeq Precision	11.77	
Elongation-at-break						
Model	233.43	5	46.685	14.89	0.000	Significant
A	19.31	1	19.307	6.16	0.025	
C	138.20	1	138.204	44.08	0.000	
A^2	18.91	1	21.711	6.92	0.019	
C^2	40.17	1	40.169	12.81	0.003	
AC	16.84	1	16.841	5.37	0.035	
Error	47.03	15	3.135			
Total	280.45	20				
Std. Dev.			1.771	R-Squared	0.8323	
Mean			4.070	Adj R-Squared	0.7764	
C.V.			43.51	Pred R-Squared	0.6683	
PRESS			93.0214	Adeq Precision	12.10	

Table 13: ANOVA table of statistical results for reduced response models

Source	Sum of squares	DF	Mean square	F value	P-value	$F > F_{crit}$
Density						
Model	0.24150	3	0.080499	20.35	0.000	Significant
A	0.01922	1	0.019218	4.86	0.042	
C	0.20854	1	0.208541	52.72	0.000	
C^2	0.01374	1	0.013739	3.47	0.080	
Error	0.06724	17	0.003955			
Total	0.30874	20				
Std. Dev.			0.0629	R-Squared	0.7822	
Mean			0.848	Adj R-Squared	0.7438	
C.V.			7.42	Pred R-Squared	0.6948	
PRESS			0.0942165	Adeq Precision	11.73	
Hardness						
Model	658.82	3	219.61	16.37	0.000	Significant
A	33.93	1	33.93	2.53	0.130	
C	568.82	1	568.82	42.40	0.000	
A^2	56.06	1	56.06	4.18	0.057	
Error	228.05	17	13.41			
Total	886.87	20				
Std. Dev.			3.66	R-Squared	0.7429	
Mean			66.3	Adj R-Squared	0.6975	
C.V.			5.52	Pred R-Squared	0.5670	
PRESS			384.055	Adeq Precision	6.969	
Surface roughness						
Model	155.165	3	51.7216	3.71	0.032	Significant
B	0.551	1	0.5513	0.04	0.845	
C	91.203	1	91.2025	6.55	0.020	
BC	63.411	1	63.4110	4.55	0.048	
Error	236.883	17	13.9343			
Total	392.048	20				
Std. Dev.			3.73287	R-Squared	0.3958	
Mean			22.3383	Adj R-Squared	0.2892	
C.V.			16.7106	Pred R-Squared	0.0226	
PRESS			383.193	Adeq Precision	5.836	

Table 13 (cont.): ANOVA table of statistical results for reduced response models

4.4 OPTIMIZATION

4.4.1 Obtaining optimum parameters

The parameter settings to optimize each response were obtained from the reduced quadratic models previously described. Table 14 describes the target value for each response, the settings for each parameter in order to achieve the target, the predicted response value, the standard error fit, and the 95% confidence interval for the response.

	Response	Target	X_1	X_2	X_3	Predicted	SE Fit	95% CI	
Y_1	Tensile strength, *MPa*	Maximize	28	7	0.006	47.06	3.43	39.79	54.32
Y_2	Tensile modulus, *MPa*	Maximize	20	7	0.006	1,497	116	1,250	1,743
Y_3	Elongation-at-break, *%*	Maximize	28	7	0.006	10.64	0.949	8.613	12.658
Y_4	Density, g/cm^3	Maximize	28	7	0.007	0.983	0.0261	0.928	1.038
Y_5	Hardness	Maximize	28	7	0.006	74.67	1.59	71.33	78.02
Y_6	Surface roughness, μm	Minimize	28	7	0.006	17.84	1.89	13.85	21.82

Table 14: Parameter settings to optimize individual responses

4.4.2 Confirmatory test

A confirmation test to demonstrate the fit of each reduced response model was performed. The target values, settings, predicted results, experimental results and typical metric values are shown in Table 15. The typical metrics are referenced from the material specification sheet for ALM PA 650, which were achieved with virgin ALM PA 650 using the processing parameters outlined in the ALM Material Processing Guide [22]. These metrics provide a baseline for comparing predictive modeling and experimental results.

	Response	Target	X_1	X_2	X_3	Predicted	Experimental	Typical [22]
Y_1	Tensile strength, *MPa*	Maximize	28	7	0.006	47.06	45.29	48
Y_2	Tensile modulus, *MPa*	Maximize	20	7	0.006	1,497	1,511	1,700
Y_3	Elongation-at-break, *%*	Maximize	28	7	0.006	10.64	5.70	24
Y_4	Density, g/cm^3	Maximize	28	7	0.007	0.980	0.973	1.02
Y_5	Hardness	Maximize	28	7	0.006	74.67	74.68	73
Y_6	Surface roughness, μm	Minimize	28	7	0.006	17.84	17.16	-

Table 15: Predicted and experimental results of confirmation tests for individual models

Ultimate tensile strength

The model for ultimate tensile strength predicted an optimal value of 47.06 MPa, which is within the range of the typical metric achieved. The experimental results showed the average ultimate tensile strength of 10 tensile bars to be 45.29 MPa, which is within the 95% confidence interval of the model. Thus, the experimental results agree well with the predicted response value.

Tensile modulus

The model for tensile modulus predicted an optimal value of 1,497 MPa. The experimental results showed the average tensile modulus of 10 tensile bars to be 1,511 MPa, which is within the 95% confidence interval of the model. Thus, the experimental results agree well with the predicted response value.

Elongation-at-break

The model for elongation-at-break predicted an optimal value of 10.64 %, which is well below the typical metric achieved with virgin ALM PA 650. The experimental results showed the average elongation-at-break of 10 tensile bars to be 5.70 %. Thus, the

experimental results disagree with the predicted response value. The discrepancy between the predicted model response and the experimental results is likely attributed to the fact that there is no correlation between strength that guarantees ductility, as shown in Figure 14 and Figure 15, taken from [31]. Thus, although the DOE methodology produced a model from the data, there is no guarantee that the model can accurately predict the response for future experiments. This is due largely to the fact that elongation-at-break is a mechanical property that is very sensitive to defects and any significant void or defect within the part will reduce the ductility of the material.

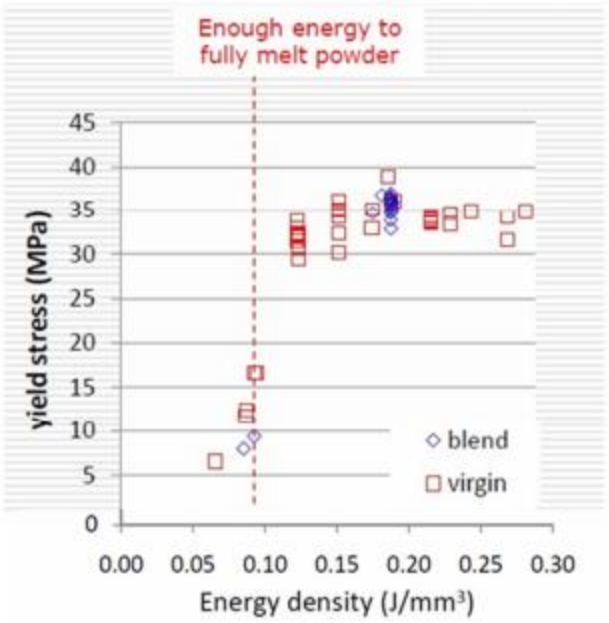

Figure 14: Yield stress versus energy density [31]

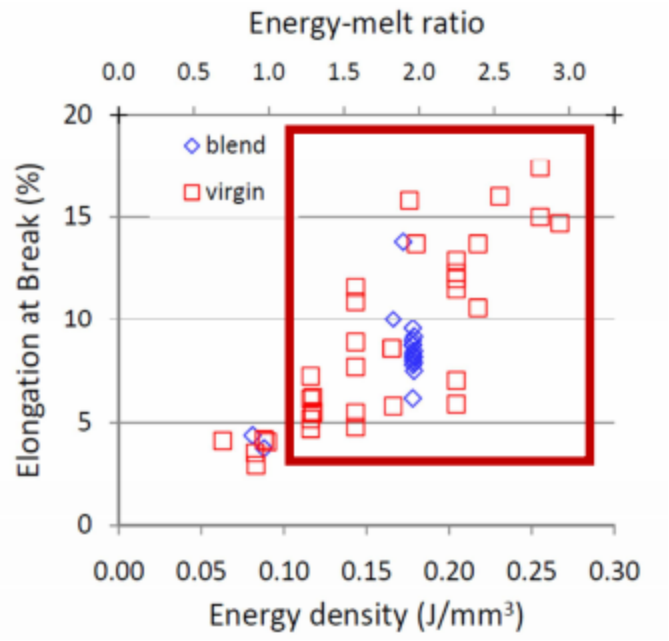

Figure 15: Elongation-at-break versus energy density [31]

Density

The model for density predicted an optimal value of 0.983 g/cm^3. The experimental results showed the average density of 5 cube specimens to be 0.973 g/cm^3, which is within the 95% confidence interval of the model. Thus, the experimental results agree well with the predicted response value.

Hardness

The model for hardness predicted an optimal value of 74.67, which is within the range of the typical metric achieved. The experimental results showed the average hardness of 5 cube specimens to be 74.68, which is within the 95% confidence interval of the model. Thus, the experimental results agree well with the predicted response value.

Surface roughness

The model for surface roughness predicted an optimal value of 17.84 µm. The experimental results showed the average surface roughness of 5 specimens to be 17.16 µm, which is within the 95% confidence interval of the model. Thus, the experimental results agree well with the predicted response value.

Chapter 5: Conclusion

5.1 SUMMARY

In this work, a DOE based methodology to optimize mechanical properties of laser-sintered parts is proposed and an application of the methodology is tested. The details of the methodology are discussed including the motivation for selecting the design variables (fill laser power, outline laser power, scan spacing), response variables (ultimate tensile strength, tensile modulus, elongation-at-break, density, hardness, surface roughness), work material (ALM PA 650 unfilled nylon 12 polyamide blend), number of experiments (21) and order of experiments (randomized). The testing methods for data collection are described and the results are presented.

Quadratic models and reduced models for each response variable are developed from the data and presented. ANOVA is performed on both full-quadratic and reduced models to determine statistical significance. Finally, a confirmation test for the optimized setting for each response variable is performed and the results are presented.

The confirmatory tests show that in all cases, with the exception of elongation-at-break, the reduced models predicted the response variables at the optimal parameter settings within a 95% confidence interval. The model for elongation-at-break (Equation 8) is not an accurate predictor for the response, which can be explained by results of previous research that demonstrated the lack of correlation between strength of the material and ductility of the material [31]. Consequently, ultimate tensile strength and tensile modulus are not good measures for the integrity of the parts.

5.2 FUTURE WORK

The work conducted within this thesis demonstrated that a model could be developed from an experimental dataset and applied to optimize a mechanical property.

The optimal settings were most often determined to be on the edge of the working range of the input parameters, thus indicating that this range should have been wider. The optimal settings for each model were the optimums within the experimental data set, however further work could focus on determining the true optimum within a wider range of the input parameter settings. Further, the optimization work that was conducted focused on maximizing or minimizing a specific property rather than aiming for a target value. Additional work could be conducted to verify validity of the models when the goal of the optimization is not a maximum or minimum value.

The work demonstrated within showed that an applicable model could be developed for the mechanical properties of tensile strength, tensile modulus, density, hardness and surface roughness. The work demonstrated that the model was invalid for elongation-at-break. Further work could be conducted to develop a set of mechanical properties for which this methodology could be applicable.

As new powder materials are developed for laser sintering, future research should implore the methodology described within in order to characterize the processing range for desired mechanical properties.

References

[1] C. R. Deckard, "Method and apparatus for producing parts by selective sintering". United States Patent US4863538 A, 17 October 1986.

[2] I. Gibson, D. Rosen and B. Stucker, "Additive Manufacturing Technologies: 3D Printing, Rapid Prototyping, and Direct Digital Manufacturing," New York, Springer, 2015.

[3] "Laser Sintering," [Online]. Available: http://www.me.vt.edu/dreams/laser-sintering/. [Accessed 20 September 2016].

[4] Objective3D Direct Manufacturing, "Laser Sintering," [Online]. Available: http://www.direct3dprinting.com.au/products/laser-sintering/. [Accessed 10 October 2016].

[5] J. C. Nelson, "Selective Laser Sintering: A definition of the process and an empirical sintering model," The University of Texas at Austin, Austin, TX, 1993.

[6] M. M. Savalani, L. Hao, P. M. Dickens, Y. Zhang., K. E. Tanner and R. A. Harris, "The effects and interactions of fabrication parameters on the properties of selective laser sintered hydroxyapatite polyamide composite biomaterials," *Rapid Prototyping Journal,* vol. 18, no. 1, pp. 16-27, 2012.

[7] T. L. Starr, T. J. Gornet and J. S. Usher, "The effect of process conditions on mechanical properties of laser-sintered nylon," *Rapid Prototyping Journal,* vol. 17, no. 6, pp. 418-423, 2011.

[8] Y. Khalil, A. Kowalski and N. Hopkinson, "Influence of energy density on flexural properties of laser-sintered UHMWPE," *Additive Manufacturing,* vol. 10, pp. 67-75, 2016.

[9] D. Bourell, J. Coholich, A. Chalancon and A. Bhat, "Evaluation of energy density measures and validation for powder bed fusion of polyamide," *CIRP Annals Manufacturing Technology,* vol. 1, no. in press, 2017.

[10] I. Gibson and D. Shi, "Material properties and fabrication parameters in selective laser sintering process," *Rapid Prototyping Journal,* vol. 3, no. 4, pp. 129-136, 1997.

[11] H. C. H. Ho, I. Gibson and W. L. Cheung, "Effect of energy density on morphology and properties of selective laser sintered polycarbonate," *Journal of Materials Processing Technology,* vol. 89, no. 90, pp. 204-210, 999.

[12] H. Zarringhalam, N. Hopkinson, N. F. Kamperman and J. J. de Vlieger, "Effects of processing on microstructure and properties of SLS Nylon 12," *Materials Science and Engineering A,* vol. 435, no. 436, pp. 172-180, 2006.

[13] C. Majewski and N. Hopkinson, "Effect of section thickness and build orientation on tensile properties and material characteristics of laser sintered nylon-12 parts," *Rapid Prototyping Journal,* vol. 17, no. 3, pp. 176-180, 2011.

[14] B. Caulfield, B. E. McHugh and S. Lohfeld, "Dependence of mechanical properties of polyamide components on build parameters in the SLS process," *Journal of Materials Processing Technology,* vol. 183, no. 1-3, pp. 477-488, 2007.

[15] T. J. Choren, V. Gervasi, T. Herman, S. Kamara and J. Mitchell, "SLS powder life study," Solid Freeform Fabrication Symposium, Austin, TX, 2001.

[16] H.-T. Liao and J.-R. Shie, "Optimization on selective laser sintering of metallic powder via design of experiments method," *Rapid Prototyping Journal,* vol. 13, no. 3, pp. 156-162, 2007.

[17] H. Chung and S. Das, "Processing and properties of glass bead particulate-filled functionally graded Nylon-11 composites produced by selective laser sintering," *Materials Science and Engineering A,* vol. 437, pp. 226-234, 2006.

[18] F. Liu, B. Zhang, C. Yan and Y. Shi, "The effect of processing parameters on characteristics of selective laser sintering dental glass-ceramic powder," *Rapid Prototyping Journal,* vol. 16, no. 2, pp. 138-145, 2010.

[19] A. K. Singh and R. S. Prakash, "DOE based three-dimensional finite element analysis for predicting density of a laser-sintered part," *Rapid Prototyping Journal,* vol. 16, no. 6, pp. 460-467, 2010.

[20] J. K. Telford, "A brief introduction to design of experiments," *John Hopkins APL Technical Digest,* vol. 27, no. 3, pp. 224-232, 2007.

[21] J. D. Williams and C. R. Deckard, "Advances in modeling the effects of selected parameters on the SLS process," *Rapid Prototyping Journal,* vol. 4, no. 2, pp. 90-100, 1998.

[22] L. Advanced Laser Materials, "Material Specifications: PA 650," 28 February 2013. [Online]. Available: http://alm-llc.com/Tech_Data_Sheets/PA_650.pdf. [Accessed 6 February 2017].

[23] ASTM Standard D638-14, "Standard Test Method for Tensile Properties of Plastics," *ASTM International,* 2015.

[24] ASTM Standard D792-13, "Standard Test Methods for Density and Specific Gravity (Relative Density) of Plastics by Displacement," *ASTM International,* 2013.

[25] ASTM Standard D2240-15, "Standard Test Method for Rubber Property—Durometer Hardness," *ASTM International,* 2016.

[26] Minitab, Inc, "What is a designed experiment?," [Online]. Available: http://support.minitab.com/en-us/minitab/17/topic-library/modeling-statistics/doe/basics/what-is-a-designed-experiment/. [Accessed 10 October 2016].

[27] Minitab, Inc, *Minitab 17 Statistical Software,* State College, PA: Minitab, Inc, 2010.

[28] Minitab, Inc, "Basics of stepwise regression," [Online]. Available: http://support.minitab.com/en-us/minitab/17/topic-library/modeling-statistics/regression-and-correlation/basics/basics-of-stepwise-regression/. [Accessed 7 4 2017].

[29] Minitab, Inc, "R-squared," [Online]. Available: http://support.minitab.com/en-us/minitab/17/topic-library/modeling-statistics/regression-and-correlation/goodness-of-fit-statistics/r-squared/. [Accessed 4 4 2017].

[30] M. Anderson and P. Whitcomb, DOE Simplified, Productivity, Inc, 2000.

[31] T. Starr, T. Gornett, J. Usher and M. Sherzer, "Laser sintering of PA-11 and PA-12 for direct digital manufacturing," Solid Freeform Fabrication Symposium, Austin, TX, 2008.

[32] "Selective Laser Sintering, Birth of an Industry," 6 December 2012. [Online]. Available: http://www.me.utexas.edu/news/news/selective-laser-sintering-birth-of-an-industry. [Accessed 20 September 2016].

[33] C. Yan, Y. Shi and L. Hao, "Investigation into the differences in the selective laser sintering between amorphous and semi-crystalline polymers," *International Polymer Processing,* vol. XXVI, no. 4, pp. 416-423, 2011.

[34] J. W. Hyatt and J. S. Hyatt, "Improvement in Process and Apparatus for Manufacturing Pyroxyline". United States Patent 133229 A, 19 November 1872.

[35] N. T. Aboulkhair, N. M. Everitt, I. Ashcroft and C. Tuck, "Reducing porosity in AlSi10Mg parts processed by selective laser melting," *Additive Manufacturing,* vol. 1, no. 4, pp. 77-86, 2014.

[36] D. K. Leigh, "A comparison of polyamide 11 mechanical properties between laser sintering and traditional molding," Solid Freeform Fabrication Symposium, Austin, TX, 2012.

[37] C. E. Majewski, H. Zarringhalam and N. Hopkinson, "Effects of degree of particle melt and crystallinity in SLS nylon-12 parts," Solid Freeform Fabrication Symposium, Austin, TX, 2008.

[38] P. Zhang, S. X. Li and Z. F. Zhang, "General relationship between strength and hardness," *Materials Science and Engineering A,* vol. 529, no. 25, p. 62–73, 2011.

[39] H. Zarringhalam, N. Hopkinson, N. F. Kamperman and J. J. de Vlieger, "Effects of processing on microstructure and properties of SLS Nylon 12," *Materials Science and Engineering A,* vol. 435, no. 436, pp. 172-180, 2006.

Vita

Lauren Violet Milisits was born in Pittsburgh, Pennsylvania. She attended Carnegie Mellon University (CMU) for her undergraduate studies. She graduated from CMU with a Bachelor of Science in Mechanical Engineering in December 2013 and a Bachelor of Science in Computer Science in May 2014. After graduation, she moved to Austin to work as a Test Automation Engineer with Spiceworks. She enrolled at the University of Texas at Austin in August 2015 to pursue a Master of Science in Mechanical Engineering and graduated in May 2017 with her degree. As of September 2017, Lauren is employed as a Pipeline Engineer with Royal Dutch Shell. She currently resides in Houston, Texas.

Email: lauren.milisits@gmail.com

This thesis was typed by the author.